2015

The Simulation & Evaluation of Surge Hazard Using a Response Surface Method in the New York Bight

Michael H. Bredesen
University of North Florida, h.bredesen@unf.edu

The Simulation & Evaluation of Surge Hazard Using a Response Surface Method in the New York Bight

Written By

Michael Hunter Bredesen

A thesis submitted to the School of Engineering in conformity with the requirements for the degree of

Master of Science in Civil Engineering

University of North Florida

College of Computing, Engineering, & Construction

April, 2015

The thesis “The Simulation & Evaluation of Surge Hazard Using a Response Surface Method in the New York Bight” submitted by Michael Hunter Bredesen in partial fulfillment of the requirements for the degree of Master of Science in Civil Engineering has been

Approved by the thesis committee: Date:

_____ _____

Donald T. Resio, Ph.D., P.E.
Thesis Advisor and Committee Chairperson

_____ _____

Christopher J. Bender, Ph.D., P.E.

_____ _____

Thobias Sando, Ph.D., P.E.

Accepted for the School of Engineering:

_____ _____

Murat Tiryakioglu, Ph.D., CQE
Director of the School of Engineering

Accepted for the College of Computing, Engineering, and Construction:

_____ _____

Mark A. Tumeo, Ph.D., P.E.
Dean of the College of Computing, Engineering, and Construction

Accepted for the University of North Florida:

_____ _____

John Kantner, Ph.D.
Dean of the Graduate School

DEDICATION

This work is dedicated to my loving sister, who I miss more than words can express.

Jenna Breanne Bredesen

July 23rd, 1985 – July 24th, 2012

ACKNOWLEDGEMENTS

I would like to take this opportunity to thank the people who helped me in my pursuit of a Master of Science degree in Coastal Engineering, which is a great accomplishment and milestone in my career. After graduating from the University of North Florida (UNF) in April 2012 with a Bachelor of Science in Civil Engineering degree, Dr. Don Resio and Taylor Engineering, Inc. (Taylor) offered me a position at the Taylor Engineering Research Institute to study coastal engineering at UNF. I would like to thank all of you for this and for showing continuous generosity and support.

Secondly, I want to acknowledge my thesis committee, Dr. Don Resio, Dr. Christopher Bender, and Dr. Thobias Sando for our technical exchanges and your extensive discussions with me throughout this process. I would not have completed this thesis without the insight and past experience that all of you have passed on to me. Special acknowledgements also go to Dr. Resio for the substantial help you provided me with your remarkable meteorological and coastal engineering knowledge; Taylor for providing the ADCIRC model for synthetic simulation; and Dr. Peter Bacopoulos and Terry Smith for assisting in the modeling process.

Next, I would like to show appreciation for my family. I am truly blessed to have such a wonderful mother and father, Sandee and Mike Bredesen. Thank you for supporting me throughout my entire life, not just during school. Without the support that both of you have given

to me, none of this would be possible. I owe you everything for this, and I love you for being kind, loving, and generous parents. I am so fortunate to have such a great life, which would not have been possible without wonderful people like you.

Lastly, even though you are not currently my official family, I wish to acknowledge my "second family." I want to thank Amanda Tancreto, as you have been my loving girlfriend for over four years, over which you have endured this process with me. I am very grateful for the love and support you give to me, and I am so lucky to have someone as special as you. Also, Glenn, Linda, and Christina Tancreto have also welcomed me into your home and family on many occasions over the past four-plus years. Thank you for the overwhelming support that you all have showed me over this time, even though I am not your own.

LIST OF CONTENTS

LIST OF FIGURES

LIST OF TABLES

List of Acronyms

ADCIRC.....Advanced Circulation

AEP.....Annual Exceedance Probability

BT.....Best Track

Cat.....Category

ccw.....Counterclockwise

CCDF.....Complementary Cumulative Probability Distribution Function

CDF.....Cumulative Probability Distribution Function

ERF.....Error Function

EST.....Empirical Simulation Technique

FEMA.....Federal Emergency Management Agency

FIRMs.....Flood Insurance Rate Maps

hPa.....Hectopascals

HPC.....High-Performance Computing

HURDAT2.....Revised Hurricane Database

JPM.....Joint Probability Method

JPM-RS.....Joint Probability Method utilizing Response Surfaces

km.....Kilometer(s)

m/s.....Meter(s) Per Second

m.....Meter(s)

MSL.....Mean Sea Level Vertical Datum

N.....North

NOAA.....National Oceanic & Atmospheric Administration

NY.....New York

NYB.....New York Bight

OS.....Optimal Sampling

PDF.....Probability Density Function

RII.....Region II

QA/QC.....Quality Assurance/Quality Control

RS.....Response Surface

TC.....Tropical Cyclone

TS.....Time Series

US.....United States

WSE.....Water Surface Elevation

NOTATION

A_0.....Gumbel Location Parameter

A_1.....Gumbel Scale Parameter

β.....Pressure Profile Parameter

C_p.....Central Pressure

°.....Degree

ΔP.....Pressure Differential

f.....Gumbel Cumulative Distribution Function

l.....Length

λ.....Poisson Frequency

μ_θ.....Heading Mean

μ_s.....Mean Surge Duration

n.....Sample Size

η.....Arbitrary Water Surface Elevation

η_{max}.....Annual Maximum Surge Level

$\eta(t)$.....Time Varying Water Surface Elevation

$\eta_{th,max}$.....Theoretical Maximum Surge Level

η_{total}.....Combined Surge & Tide Water Surface Elevation

η_*.....Combined Tropical Cyclone Characteristics

$\eta_{\#}$.....Synthetic Tropical Cyclone's Water Surface Elevation

η_{*}''.....Water Surface Elevation for Constant Velocity

η_{+}.....Mean Displacement Due to Tidal Oscillation

R_m.....Radius to Maximum Winds

ψ.....Latitude

θ.....Tropical Cyclone's Relative Angle of Incidence to the Shoreline

θ_{edge}.....Angle Band Edge

$\widehat{\sigma}$.....Average Surge Standard Deviation

$\sigma_{\ln(R_m)}$.....Log-Normal Tropical Cyclone Size Standard Deviation

σ_{tide}.....Standard Deviation of Random Tidal Oscillation Displacement

σ_{θ}.....Tropical Cyclone Heading Standard Deviation

σ_s.....Average Half-Surge Duration

σ_{τ}.....Additional Flood Contribution Term

$\sigma_{\tau_{mod}}$.....Standard Deviation of Uncertainty Due to Model Error

σ_{τ_s}.Standard Deviation of Uncertainty Due to Suppression of Natural Tropical Cyclone Variation

T_{η}.....Return Period

t_{peak}.....Time of Maximum Theoretical Surge

t_s.....Sample Period

t_{srg}.....Average Surge Duration

$\hat{t}$.....Normal Distribution Half-Time

τ.....Additional Flood Contribution Term

τ_{mod}.....Uncertainty Due to Model Error

τ_s.....Uncertainty Due to Suppression of Tropical Cyclone Natural Variation

τ_{tide}.....Uncertainty Due to Tidal Oscillation

V_f.....Tropical Cyclone Forward Velocity

X.....Tropical Cyclone Location

Z_{R_m}.....Log-Normal Random Variable Z for Tropical Cyclone Size

$Z_{\theta_{edge}}$.....Log-Normal Random Variable Z for Angle Band Edge

ABSTRACT

Atmospheric features, such as tropical cyclones, act as a driving mechanism for many of the major hazards affecting coastal areas around the world. Accurate and efficient quantification of tropical cyclone surge hazard is essential to the development of resilient coastal communities, particularly given continued sea level trend concerns. Recent major tropical cyclones that have impacted the northeastern portion of the United States have resulted in devastating flooding in New York City, the most densely populated city in the US. As a part of national effort to re-evaluate coastal inundation hazards, the Federal Emergency Management Agency used the Joint Probability Method to re-evaluate surge hazard probabilities for Flood Insurance Rate Maps in the New York – New Jersey coastal areas, also termed the New York Bight. As originally developed, this method required many combinations of storm parameters to statistically characterize the local climatology for numerical model simulation. Even though high-performance computing efficiency has vastly improved in recent years, researchers have utilized different "Optimal Sampling" techniques to reduce the number of storm simulations needed in the traditional Joint Probability Method. This manuscript presents results from the simulation of over 350 synthetic tropical cyclones designed to produce significant surge in the New York Bight using the hydrodynamic Advanced Circulation numerical model, bypassing the need for Optimal Sampling schemes. This data set allowed for a careful assessment of joint probability distributions utilized for this area and the impacts of current assumptions used in deriving new flood-risk maps for the New York City area.

Chapter 1

INTRODUCTION

The earth and its atmosphere are a continually changing dynamic system. Earth's air, for instance, is constantly driven by the globe's rotation on its axis, its revolution around the sun, and the transfer of energy from the sun (Tarbuck & Lutgens, 2006). Solar energy heats the earth unevenly due to the planet's motions. This non-uniform energy distribution induces constantly shifting circulation patterns, which manifest themselves in the form of winds. The energy transfer process continues into the earth's surface, where sporadic heating from the sun assists the macro-scale water movements creating ocean currents. The aforementioned winds transfer energy into the water's surface due to friction and pressure gradients, building waves and inducing surface currents. These forces, whether large or small, continually shape earth's evolving surface features.

This evolution may be most noticeable along coastlines, where land, air, and water merge (Tarbuck & Lutgens, 2006). The world's shorelines were first primarily used for naval and commercial purposes, but have also long been recognized as an important source for recreation and tourism (Dean & Dalrymple, 2002). Coastal populations have continued to increase due to the attractiveness and utility of coastal areas. However, as beautiful as coastal areas may be, it is also a region of exacerbated hazard related to storm surges, waves, and the destruction caused by these hazards. Major storms such as "northeasters" (extratropical storms) and hurricanes,

generically known as tropical cyclones (TCs), can negatively affect human life and infrastructure along the shoreline.

1.1 Coastal Hazards

Natural coastal hazards can be broken down into two categories: long-term and short-term processes. Understanding how to quantify and efficiently mitigate the threat posed by coastal hazards is vital to the resilience of coastal communities. Long-term processes act over a period of months, years, decades, or longer. Relative sea level change forms a backdrop for coastline evolution and is directly correlated to long-term geological and climatological processes such as land subsidence and global warming. Advancing or retreating shorelines not only play an important role in the performance of manmade coastal structures, but they can also influence natural coastline features (Dean & Dalrymple, 2002). To gain a better understanding of mean sea level change, historic records of water surface elevations (WSEs) can be found that date back over 400 years in the Netherlands (Dean & Dalrymple, 2002). However, records are sparse and interpolating data can be questionable. Short-term coastal events reside on a temporal scale of days, hours, or sometimes even minutes. These types of coastal events, and more notably the hazards that result from TCs, will be the main focus of this manuscript. To gain a better understanding on how these events can affect coastal regions, a short discussion on the risk associated with noteworthy short-term processes is introduced in this section even though this article focuses on hazards rather than risk.

Atmospheric variations in the northern hemisphere's winter months can cause what are known as "northeasters," which are coastal cyclonic storms that rotate counterclockwise (ccw) in a low pressure system around a central low pressure extreme (C_p). This type of storm has historically

caused major erosional damage along the eastern seaboard of the US. Depending on the nature of the event, northeasters can impact long spans of coastline with days of wind up to 31 meters per second (m/s), waves, and currents (USGS, 2014a). The notorious 1962 Ash Wednesday northeaster impacted the Middle Atlantic states for days, spanning over five tidal cycles, causing widespread coastal erosion, and generating extensive flooding (Dean & Dalrymple, 2002). The most costly northeaster to date was the 1991 "Perfect Storm." This storm was initiated by TC Grace and ultimately transitioned into an extratropical storm, culminating in an estimated $1 billion (US) in damages along the eastern seaboard of the US and Canada (USGS, 2014a).

The most destructive coastal hazard within the US is a TC. Warm, moist ocean waters evaporate in tropical latitudes, condensing to form clouds (USGS, 2014b). Warm air continues to rise, causing C_p to drop due to less air mass at at the ocean's surface. The pressure differential (ΔP) (defined as peripheral pressure, 1013 hectopascals or hPa, minus C_p) and energy transfer from the condensation results in cooler air temperatures that blow toward the C_p (which becomes the "eye" of the newly formed storm system). The cooler air subsides slowly within the eye-wall region before rising again. This process forms winds that rotate ccw in the northern hemisphere due to the earth's rotation on its axis. The storm intensifies, using the latent heat from warm tropical waters as an energy source. This short-term process officially becomes a TC that is classified as a hurricane as wind speed reaches 33 m/s, according to the commonly used Saffir-Simpson Hurricane Scale displayed in Table 1.

Table 1: Saffir-Simpson Scale Hurricane Scale (Kantha, 2012)

Category	Central Pressure	Estimated Sustained Wind Speed	Estimated Surge	Damage Classification
-	hPa	m/s	m	-
Tropical Depression	1000 - 1007	< 17	-	-
Tropical Storm	981 - 999	17 - 32	-	-
Category 1 Hurricane	≤ 980	33 - 42	1.2 - 1.6	Minimal
Category 2 Hurricane	965 - 979	43 - 49	1.7 - 2.5	Moderate
Category 3 Hurricane	945 - 964	50 - 58	2.6 - 3.8	Extensive
Category 4 Hurricane	920 - 944	59 - 69	3.9 - 5.5	Extreme
Category 5 Hurricane	< 920	> 69	> 5.5	Catastrophic

1.1.1 TC Surge Hazard Quantification

TCs are affected by large-scale wind and pressure field variations on a scale of several days and 1000's of kilometers (km). Shear stress is developed from TC winds impacting the ocean water's surface, producing storm surge and surface wind waves that are responsible for the majority of the economic damages along coastlines (the single notable exception to this was Hurricane Andrew, which struck just south of Miami in 1992). Because there is little measured data in areas devastated by TCs, predicting inundation levels by numerically modeling storm surges has become the method of choice for developing estimates of coastal inundation hazards.

Typical requirements for these numerical simulations include designing sustainable coastal structures and implementing insurance rate maps by predicting annual exceedance probabilities (AEPs) due to flooding – normally the 1% annual chance, often called the "100-year (flood) event." Such predictions contain some level of error due to the complex nature of TCs, but establishing accurate surge hazard estimation methods are important for public safety and hazard mitigation. Technological advances have increased understanding of hurricane characteristics

and wind fields within TCs, which has led to quicker and more reliable methods for estimating the potential impact affiliated with extreme coastal events over the past decade (Irish et al., 2009). Past techniques that constructed design storms were based on historical records (tide gauge analyses), the empirical track model, the empirical simulation technique (EST), and the joint probability method (JPM) (Myers, 1975; Ho & Meyers, 1975). The work presented in this manuscript used the JPM, as it is currently accepted as the preferred technique in estimating TC surge probabilities in the US.

1.1.1.1 The JPM

Irish et al. (2011) showed the statistical JPM approach provides information on hurricane surges rather than solely using data based on historical TCs at a particular site since it covers any possible storm rather than only those that have occurred over a fixed interval. This main point describes why the JPM has become the method of choice post-Katrina for extreme-value surge analyses in the US (Song, 2012). This probability method uses the local storm climate along a stretch of coast to develop a set of storms, weighting the storms by their rate of occurrence (Toro et al., 2010b). The local climatology is based on sampling historic records by considering past storm tracks and TC parameters along those tracks. Constructed events are simulated via numerical models to compute WSEs due to that particular storm. The JPM then utilizes the synthetic maximum WSEs in conjunction with the historic annual rate of storms and the joint probability distributions of the TC parameters to generate flood elevations in excess of a certain WSE (Toro et al., 2010a). Currently, this technique yields the most precise results when used correctly, which is why the JPM was selected as the statistical approach for the work presented in this manuscript.

1.1.1.2 Surge Hazard Quantification in the Northeast US

Recent storms (including those in Figure 1) impacting the New York Bight (NYB) have resulted in devastating flooding in New York City, the most densely populated city in the US. As a part of national effort to re-evaluate coastal inundation hazards, the Federal Emergency Management Agency (FEMA) re-evaluated the Flood Insurance Rate Maps (FIRMs) in this area. FEMA's study required a thorough investigation of the coastal storm surge flood frequencies that incorporated an optimal sampling (OS) form of the JPM (FEMA, 2013). The OS scheme limits the number of simulations to reduce overall computational requirements and is further detailed later in this manuscript. The work presented herein had two main objectives: (1) quantify surge hazard in the NYB (Figure 2) using a direct JPM as opposed to the previously addressed optimal sampling JPM (JPM-OS), and (2) compare the probabilities found here versus the probabilities resulting from applying some assumptions inherent in the FEMA FIRMs to the developed storm set in the NYB – and more notably Battery Park, New York (NY). This work also aims to shed light on possibly underestimated TC surge probabilities in the NYB.

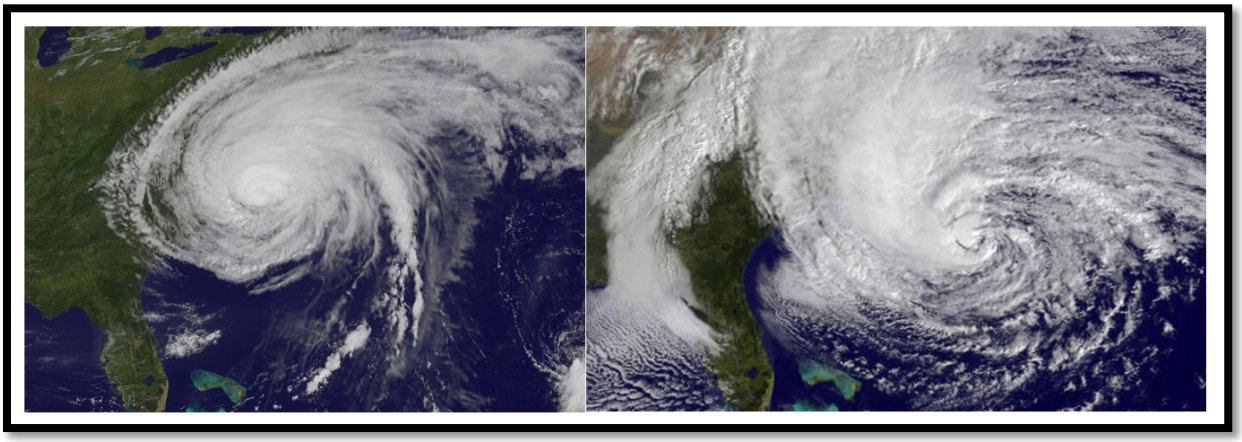

Figure 1: TCs Irene (Left) & Sandy (Right) Are Displayed Impacting the Northeast US

Figure 2: General Coastal Flood Study Area

Chapter 2

METHODOLOGY

Flood frequency analyses start with the estimation of storm hazards, which is where FEMA FIRMs commence. These maps are "the official map(s) of a community on which FEMA has delineated both the special hazard areas and the risk premium zones applicable to the community" (FEMA, 2014), and misrepresentation of the zone delineation lines could lead to significant economic impacts. The FEMA FIRMs require an estimation of maximum WSE frequencies due to storm surge by the 10-, 50-, 100-, and 500-year event flood levels (Toro, 2012). Currently, the JPM is the accepted methodology for many federal agencies' prediction of surge flood frequencies. However, some assumptions inherent in the statistics detailed in FEMA (2013) are questioned in this manuscript. The probabilities that result from those assumptions are compared with the probabilities found here to quantify the impact they may have in misestimating AEPs in the NYB.

2.1 Foundation for Approach

In short, this study consisted of seven primary steps: (1) defining the local TC climatology (and associated storm rate) from published TC databases; (2) characterizing TCs in the selected region via a synthetic storm set; (3) establishing an accurate simulation model with precise bathymetric and topographic data; (4) simulating the synthetic storm set over the range of TCs that contribute to the probabilities of interest; (5) assessing the epistemic uncertainty terms (i.e. astronomical tides, model errors, etc.); (6) evaluating response surfaces as a function of the same parameters

used to define the TCs in the storm set; and (7) comparing results published in this work to frequencies from previous analyses that employed particular assumptions in question.

2.2 Regional Geography & Climatology Overview

The general coastal flood study area shown in Figure 2 is characterized as FEMA's Region II (RII), which encompasses the coastal areas of NY (including Long Island), New Jersey, Westchester County, NY, and the banks of the tidal portion of the Hudson River (FEMA, 2013). Battery Park, NY is in a geographically vulnerable location, as it is positioned at the delta of the Hudson River, adjoining the Hudson Shelf Valley. Figure 3 displays the project area's coastline via Google Earth to adequately depict the valley in the ocean floor leading into Lower Bay. The funnel-shaped coastline has also long been known to produce higher than normal surge levels (NYC, 2014). This knowledge, coupled with the observed sea level trend of +2.83 (+/- 0.09) millimeters per year (NOAA, 2013), could lead to unprecedented destruction to the US's most densely populated city (Kay, 2014). Due to the preceding reasons, the location of Battery Park, NY was the focal point for this work.

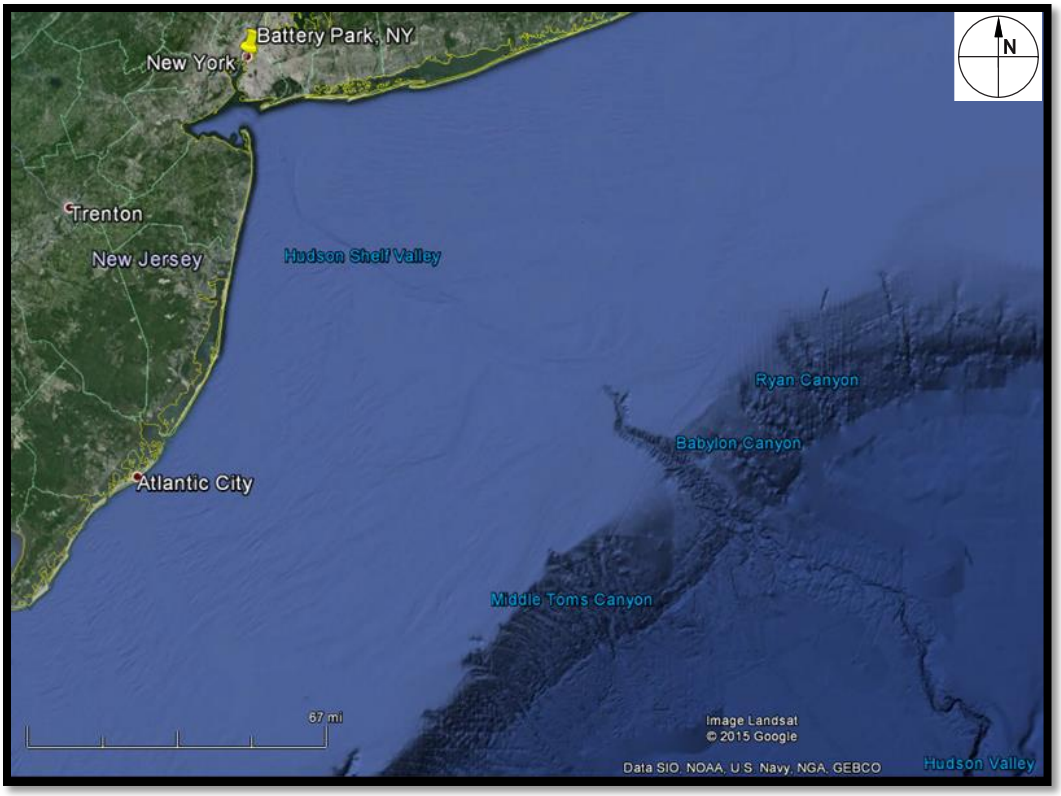

Figure 3: Representation of the Vulnerable NYB Coastline (Source: Google Earth, 2015)

2.2.1 Data Source

Defining characteristic storms for synthetic simulation may be difficult in the NYB due to sparse historical observational data. In 2014, NOAA's National Weather Service published a "revised" Atlantic hurricane database that encompassed historical TC data from 1851 to 2012, including TC Sandy (NOAA, 2014). This information is published in the National Hurricane Center's database, where a complete evaluation of the history of every developing TC (even non-developing tropical depressions) was documented (Landsea et al., 2014). The new material is known as the second generation Atlantic hurricane database (HURDAT2), which replaced the original HURDAT format developed by Jarvinen et al. (1984). HURDAT2 includes non-synoptic best track (BT) times for landfall (X)/C_p indications and wind radii, where both are based on

analyses from the Best Track Change Committee (Landsea et al., 2004a; Landsea et al., 2004b; Landsea et al., 2008; Landsea et al., 20012; Hagen et al., 2012; Landsea et al., 2014). Each parameter's statistical distribution (Table 2) was derived from HURDAT2, as the dataset provides the necessary meteorological data to sample and make up the probabilistic definition of the storm criteria for the JPM.

2.2.2 TC Characterization Overview

To complete an accurate storm surge analysis with the JPM, two general types of information are required: (1) a quantified local climatology of storms affecting an area and (2) quantified surges resulting from any possible TC, not just TCs that have happened in the past. The second point is important, as this was the downfall to some of the previous schemes when calculating surge probabilities.

2.2.2.1 TC Parameters

The JPM typically uses five or six storm parameters to develop wind fields for each parametric storm. The traditional parameters include storm intensity, storm size, storm heading (angle of incidence to the shoreline), storm track (landfall location from a fixed location, which is the same as "d" in Figure 4), and storm forward translation speed ($\Delta P/C_p$, R_m, θ, X, and V_f, respectively). These are the storm characteristics that were used in the JPM for this analysis and are displayed in Figure 4 from Toro et al. (2010a), which shows a theoretical representation of a TC nearing a coastline. One other characteristic has been shown to play a role in TC hazard prediction that is not shown in Figure 4, and it is known as Holland's B (β).

Figure 4: Portrayal of a Storm Nearing a Coastline (Source: Toro et al., 2010a)

Table 2 shows the storm parameters, associated probability distributions, and selected values for this analysis. These values were selected in a way to cover the whole scope of the local climatology with sufficient resolution, while minimizing the number of storm simulations. Because TC surge is generally known to be less sensitive to V_f in relation to C_p or R_m and have a known parametric representation for response to variations, this parameter was held constant to reduce the number of simulations needed to complete the analysis. However, a sensitivity study was performed to validate the local response to this parameter. All storm characteristics used in the JPM integral for this study are further discussed in Chapter 3.

Table 2: Storm Characteristics with Associated Distributions & Values Used

Storm Characteristic	Units	Values Used	Distribution Parameters from FEMA (2013)	Distribution Used in this Manuscript
Pressure Differential (ΔP)	Hectopascals (hPa)	920, 940, 960, 980	3-Parameter Weibull	2-Parameter Gumbel
Radius to Maximum Winds (R_m)	Kilometers (km)	27.78, 55.56, 83.34	Lognormal, Dependent On ΔP & Latitude (ψ)	Lognormal, Dependent On ΔP & Latitude (ψ)
Angle (θ)	Degrees (°) - Measured ccw from Due N	-22.5, 0, 22.5, 45	Approximately Normal, Independent	Approximately Normal, Dependent on ΔP
Storm Track (X)	Meters (m) - Perpendicular Distance from Site	-	-	-
Velocity (V_f)	Meters Per Second (m/s)	12.86*	Normal, Dependent On C_p	Approximately Normal, Independent
Holland's B (β)	Dimensionless	1.1	Normal, Dependent On R_m & ψ	Held Constant

*A sensitivity study was completed on V_f to include as a scaling function in the JPM integral

2.3 Numerical Surge Modeling

Surge, waves, and precipitation are the three main components to inundation due to TCs. Accurately quantifying possible flood levels due to these constituents can be accomplished by different computational modeling suites. A network of computer programs that solve free-surface circulation problems in a time dependent manner were used to simulate synthetic storms impacting the NYB region, which included the traditional Advanced Circulation (ADCIRC) hydrodynamic model (Luettich Jr. et al., 1992; Blain et al., 1994; Westerink & Luettich Jr. 1994). ADCIRC has been previously applied in many inundation analyses around the country, as it

allows the user to readily create an unstructured grid (or mesh) by use of the finite element method (Luettich Jr. et al., 1992). The mesh development procedure involves overlaying seamless digital elevation models with rich topographic and bathymetric datasets, which can result in fine grids and accurate WSE extremes.

A pre-calibrated ADCIRC hydrodynamic surge model was used as the surge model in this study, which was provided by Taylor Engineering, Inc. for the academic research presented here. The mesh displayed in Figure 5 contained 604,790 nodes and 1,188,640 elements. Element sizes ranged from over 100 km near the mesh boundary (in the Atlantic Ocean) to approximately 100 meters (m) in the bays and rivers along the coastline in the NYB area. The grid was referenced to the North American Vertical Datum of 1988 (NAVD88) and was horizontally projected via the North American Datum of 1983 (NAD83) Geographic Coordinate System (latitude and longitude).

In brief, the numerical modeling process consisted of five main steps: (1) validating the model's mesh; (2) completing 336 "production" simulations with pre- and post-processing quality assurance/quality control (QA/QC) procedures; (3) completing a sensitivity study with 16 additional runs to quantify the dependence of V_f; (4) removing astronomical tides assuming linear superpostition for Battery Park, NY (to be added as uncertainty in the JPM calculation); and (5) convert the resulting WSE values from NAVD88 to the Mean Sea Level (MSL) vertical datum used in this study.

Graphic redacted, paper copy available upon request to home institution.

Figure 5: The ADCIRC Model's Computational Domain

2.4 JPM Overview

The JPM follows a process that combines three different types of information: (1) the historical frequency of storms at a given stretch of coast (λ – with units of storms/degree/year), which typically follows a Poisson process; (2) the joint probability distribution of storm characteristics $P(\eta_*)$; and (3) the storm surge at a particular site of interest as a function of the storm parameters ($\eta_\#$ – with units of m), which results from a model simulation (Toro et al., 2010a). The mathematical representation of the traditional JPM is expressed by the multiple integral (E-1).

$$F(\eta_{max} > \eta) = \lambda \int \dots \int_{\eta_*} P(\eta_*) P(\eta_{\#} > \eta)\, d\eta_* \quad \text{(E-1)}$$

where

- $F(\eta_{max} > \eta)$ is the cumulative probability distribution function (CDF),
- η_{max} is the annual maximum surge level (m), and
- η is the arbitrary WSE threshold (m).

(E-1) utilized the model output extremes at Battery Park, NY to determine the portion of storms that exceeded 0.5 m (without the inclusion of natural tidal oscillations). The multiple integration results in a rate of exceedance that is converted to an AEP when multiplied by λ. Toro et al. (2010b) showed that the left side of (E-1) is actually equivalent to the complementary cumulative probability distribution function (CCDF) when evaluated specifically as a function of the flood elevation level.

Some traditionally applied techniques have used only historical records to represent storms for probability analyses. While the JPM does use historical archives from which to sample data, this method samples parameters, not storms. These parameters are then projected to yield the AEP for any possible TC event. Other schemes may not be able to properly encompass the range of characteristics needed to portray a natural event, and others are highly sensitive to sampling errors due to unsatisfactory sample sizes. On the contrary, Resio (2007) illustrated how there is no limit to the number of dimensions in the JPM, as it can handle any number of parameters necessary to characterize a TC. However, dimensionality can sometimes be problematic – more dimensions equals more characteristic combinations (which in turn results in more synthetic simulations).

As it is currently necessary to utilize higher and higher resolution maps to suffice for the most accurate accurate model simulation results, trade-offs are sometimes required when accomplishing flood frequency studies. The brute-force method of the mathematically intense JPM can require thousands of model simulations. While one storm simulation for this analysis took approximately three wall-clock hours to run on a 384 parallel CPU High-Performance Computing (HPC) Cluster, a compromise between saving time (and money) by reducing the amount of production simulations is normally required. This compromise has resulted in OS schemes that were developed in the critical post-Katrina era to allow for a smaller number of simulations while still preserving precision in the frequency analysis (Resio, 2007; Irish et al., 2009; Resio et al., 2009; etc.).

The term “optimal” conveys a balance between simulation costs and resulting accuracy. The two OS schemes that have been adopted in flood frequency studies in the past were (1) JPMs exercising a Bayesian Quadrature (Toro et al., 2010b) and (2) JPMs applying Response Surface (RS) functions (JPM-RS) (Resio, 2007; Irish et al., 2009; Irish et al. 2009). The Bayesian quadrature technique samples a small number of storms and appropriately loads each simulation to yield a weighted summation. The JPM-RS can also use an OS approach. This method interpolates between surge results from the judiciously selected storms simulated via numerical models. Both methods have proven to yield accurate AEPs (while minimizing the efforts of the traditional JPM by approximately an order of magnitude), and variation in the results between the two have proven to be minimal (Toro et al., 2010b). This analysis applied the JPM-RS scheme without the need for OS to predict inundation probabilities of exceedance for the NYB area, focusing on Battery Park, NY.

2.4.1 Additional Flood Contributions

In all simulations of complex natural phenomena, some sort of error is inherent in the results. Knowing the degree of a study's validation is important to accurately represent TC AEPs, as the effect of uncertainty on TC surge hazard estimates have shown to be significant (Resio et al., 2013). Quantifying the additional flood contributions in this study was completed by incorporating two different types of error classes: (1) random deviations in nature not captured in the techniques used and (2) bias in the resulting AEPs due to known deviations not captured by the JPM. These components were added to the integral in (E-1), represented by the tau term (τ) in (E-2).

$$F(\eta_{\max} > \eta) = \lambda \int \dots \int P(C_p, R_m, \theta, X, V_f) P(\eta_{\#} + \tau > \eta)\, dC_p dR_m d\theta dX dV_f d\tau \quad \text{(E-2)}$$

Chapter 3

TC Characterization & Synthetic Simulation

Historical TC data have improved greatly in the past 60 to 70 years due to evolving record-keeping techniques. Figure 6 from McAdie et al. (2009) shows the progress and approximate dates of the technological advancements of observational schemes. These advancements have led to modern data collection, where Landsea et al. (2004a; 2004b; 2008; and 2012) attempted to maximize the consistency of all storms (by use of all Figure 6 techniques and some not listed) to make up a unified TC dataset in the HURDAT2 record.

Figure 6: TC Observational Technique Dates (Source: McAdie et al., 2009)

3.1 Period of Record

The HURDAT2 records range from the period 1851 – 2012. However, Landsea et al. (2014) noted that this archive is far from complete or entirely accurate. TC data in this archive become more infrequent the further back in time a sample is taken from. However, researching the history of the landfalling TCs was necessary to insure inclusion of historically important storms that impacted the NYB. An example of an older but very important storm is the infamous Great New England Hurricane of 1938. This event resulted in maximum WSEs of 4.27 – 5.49 m and 5.49 m – 7.62 m across much of the Connecticut and Massachusetts coastlines, respectively (NOAA, 2005), and was responsible for an estimated 684 deaths and over $300 million (US in 1938) in damages (Scotti, 2003). The analysis performed here considered all storms in the HURDAT2 records from 1930 – 2012, resulting in a sample period of 83 years.

3.1.1 TC Sample

On one hand, sparse data representing TCs (especially very intense ones) limit the characterization of natural events for the JPM integration, which motivates a sample to be taken over a large spatial area. On the other hand, Niedoroda et al. (2010) points out that expanding a search zone could misrepresent TC characteristics at a particular location (such as Battery Park, NY) due to spatial inhomogeneity. As a compromise to both considerations, TC characteristics for this study were found via sampling a zone bounded by (75.5° W, 38.5° N), (72.0° W, 38.5° N), (74.0° W, 41.0° N), and (71.0° W, 41.0° N), represented in Figure 7 by the corners of the trapezoidal box. Based on the distribution parameters presented in Vickery &Wadhera (2008), 980 hPa was utilized as the upper limit of C_p in the sample. The sampled storms and their associated parameters are listed in chronological order in Table 3.

Table 3: Storms Sampled from the HURDAT2 Dataset at Lowest Pressure

Storm Name	Storm Date	Central Pressure	Velocity	Angle - ccw from due N
-	Year	hPa	m/s	°
Unnamed*	1938	940	7.202	-2.8
Esther	1961	972	3.006	-26.6
Agnes	1972	980	10.356	8.5
Belle	1976	977	11.555	-10.3
Bob	1991	953	13.730	-32.0
Floyd	1996	980	18.232	-39.8
Floyd	1999	980	15.111	-34.7
Irene	2011	959	1.592	-24.8
Sandy	2012	943	0.650	58.0

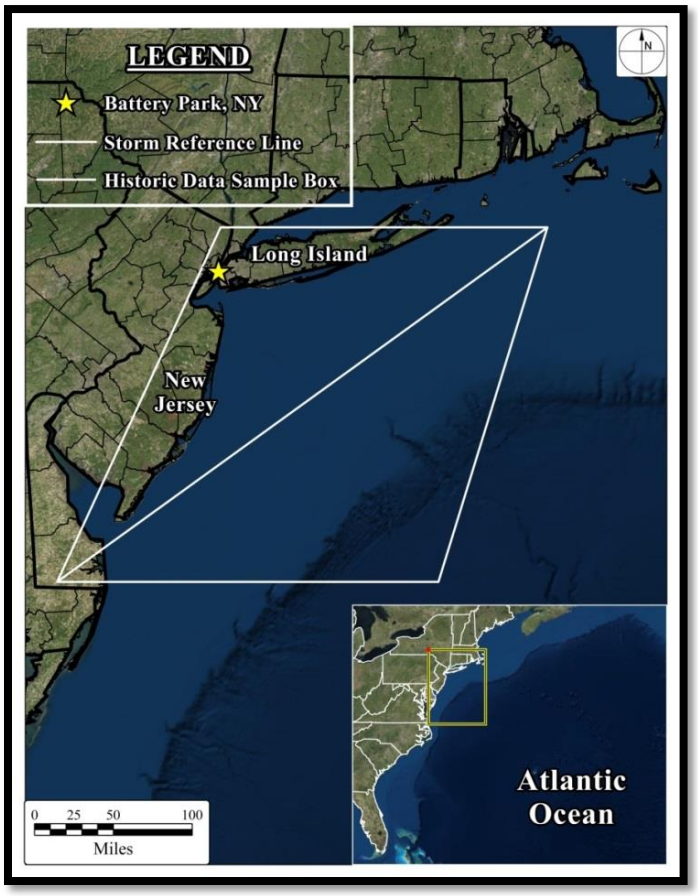

Figure 7: Data Sample Box & Reference Line for the Track-Crossing Method

3.1.2 TC Frequency

TC surge studies typically assume that storm rates can be represented by a stochastic Poisson process. This work utilized a similar approach to calculating the historical TC frequency in the NYB, where a track-crossing method was adopted for sampling storms in this analysis. Figure 7 shows the reference line that was used in the track-crossing method, measuring a total of 4.69° from the southwestern to northeastern corners of the sample box. This resulted in a storm rate of approximately 2.31×10^{-2} storms/degree/year by using (E-3).

$$\lambda = \frac{n}{l * t_s} \quad \text{(E-3)}$$

where

- λ is the storm rate following a Poisson distribution (storms/degree/year),
- n is the number of storms in the resulting sample (storms),
- l is the length of the reference line (°), and
- t_s is the period of the sample (years).

3.2 TC Parameters

The JPM utilizes a set of parametric storm characteristics, where the likelihood of a storm occurring by a certain combination of parameters is defined by the statistics of those parameters (Niedoroda et al., 2010). The basic parameter set for simulations in this study consisted of four main parameters (C_p, R_m, θ, and X), with each of these characteristics covering a fixed range of values with evenly spaced increments. TC forward velocity (V_f) and the pressure profile parameter (β) were held constant for all production simulations.

Characterizing Atlantic TCs by offshore values compared to landfall values is also of concern in surge studies. TCs usually tend to "fill" before landfall, meaning a decrease in storm intensity by a relative change in the values of parameters. Resio (2007) documented that normal pre-landfall TC filling occurs when the storm traverses the final 167 km prior to landfall in the central Gulf of Mexico region. Because the surge response is typically largest within this period, evaluating a storm by landfall characteristics is usually deemed necessary. However, FEMA (2013) noted that within the 30 storms sampled in the analysis used for the NYB area, no pre-landfall filling was observed. This analysis also assumed that pre-landfall storm decay is minimal in this area, which could result in an over-estimate in AEPs and form a basis for future work.

3.2.1 TC Central Pressure Deficit

The response surface method utilizes ΔP and R_m as the two main parameters in the multidimensional integration because a TC's surge response has been shown to be largely encompassed by the variation of these two characteristics (Irish et al., 2008). ΔP is statistically well described by a three-parameter Weibull distribution when sample sizes are sufficient (Niedoroda et al., 2010). However, because the curvature term is sensitive to the number of storms sampled and historical records only produced nine storms with the criterion listed in 3.1, a two-parameter Gumbel distribution was utilized here. The input data from the historical storms are listed in Table 4 and the Gumbel CDF is shown by (E-4).

Table 4: Input Data for Gumbel Distribution

Storm	Rank	ΔP	Estimated Return Period
Agnes	1	33	10.25
Floyd	2	33	11.53
Floyd	3	33	13.17
Belle	4	36	15.37
Esther	5	41	18.44
Irene	6	54	23.06
Bob	7	60	30.74
Sandy	8	70	46.11
Unnamed	9	73	92.22

$$f = e^{-e^{-(Z_G)}} \quad \text{(E-4)}$$

where

- f is the Gumbel CDF.

and

$$Z_G = \frac{\Delta P - A_0}{A_1} \quad \text{(E-5)}$$

where

- A_0 is the Gumbel location parameter, found to be 40.284, and
- A_1 is the Gumbel scale parameter, found to be 15.969.

The four C_p's used to make up the synthetic storm set deviated by an even 20 hPa and ranged from 980 (weakest) to 920 (strongest) hPa. The ΔP range of 33 – 93 hPa resulted from simply subtracting the peripheral pressure (typical sea surface pressure of 1013 hPa) from the respective

C_p value. Figure 8 shows the sampled storms and the best-fit Gumbel distribution of ΔP, represented by the double log of the Gumbel CDF.

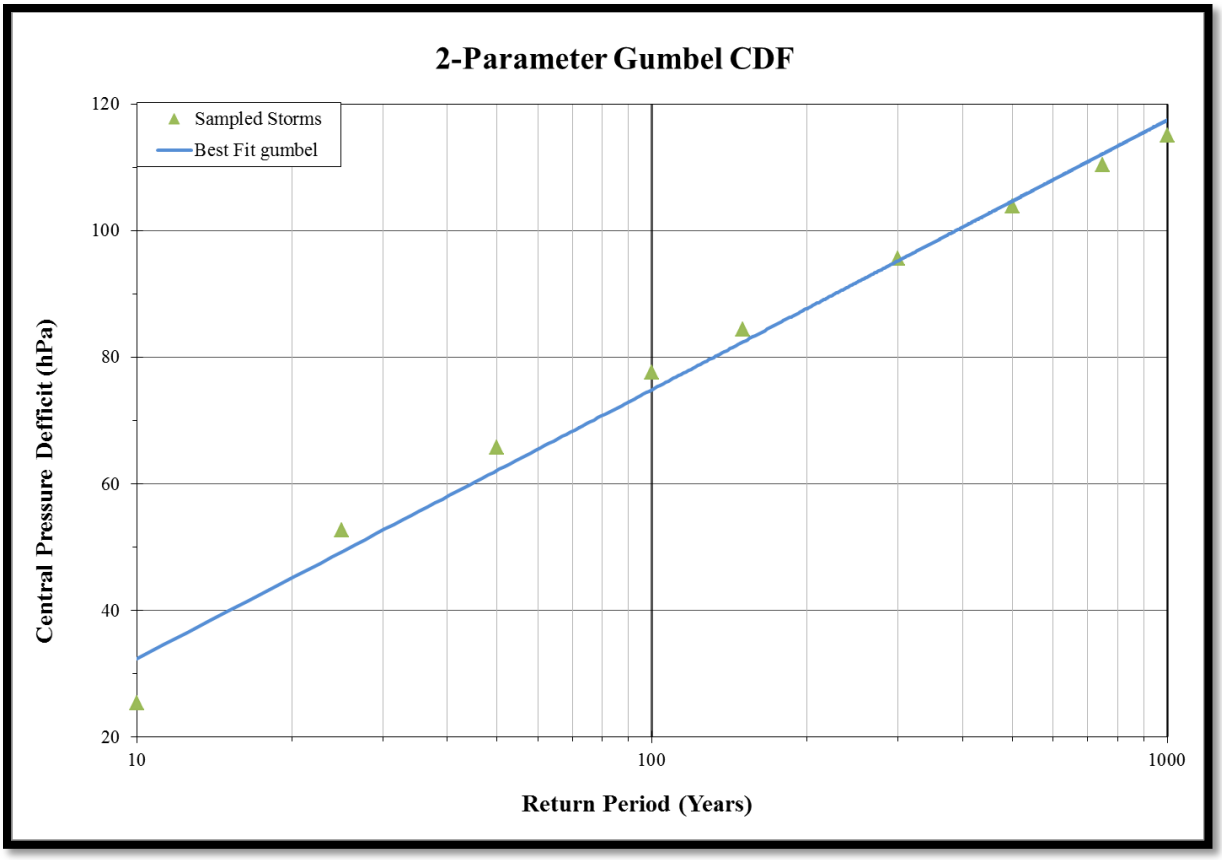

Figure 8: Best-Fit Gumbel CDF for Sampled Storms with $\Delta P \geq 33$ hPa

3.2.2 TC Size

Vickery & Wadhera (2008) utilized all available flight-level pressure and wind records from reconnaissance aircrafts from the period 1977 – 2001 to draw samples and test the correlation of the R_m parameter to other TC characteristics. That study found that the R_m to ΔP model had a coefficient of determination (statistical R^2 value) of only 0.297. Even though this indicates these two parameters are not well correlated, they are the two most important characteristics that define TC surge in the JPM-RS space. Assuming statistical dependence ensures very low C_p

values are not assigned to very high R_m values in the synthetic storm set (Toro, 2012). Therefore, the statistics presented within Vickery & Wadhera (2008) were used in this analysis, which showed that R_m is best fit with a log-normal distribution and assumed to be correlated with ΔP and latitude (ψ) (E-6).

$$\ln\left(R_{m,med}\right) = 3.015 - (6.291 \times 10^{-5}) * \Delta P^2 + 0.0337\,\psi \quad \text{(E-6)}$$

where

- ψ is latitude taken to be 40.7° (taken to be the ψ near the site of interest, somewhat offshore).

Because the distribution was assumed to be log-normally distributed, the CDF was evaluated with a logarithmic error function (ERF) at the mid-points of the evenly spaced R_m intervals used to statistically describe TC size in the NYB: (1) 27.78 km, (2) 55.56 km, and (3) 83.34 km. The ERF was evaluated at $\frac{Z_{R_m}}{\sigma_{\ln(R_m)}\sqrt{2}}$, where the standard deviation ($\sigma_{\ln(R_m)}$) was found to be 0.441 for all Atlantic TCs (Vickery & Wadhera, 2008). The subsequent CDF equation is displayed in (E-7), where Z_{R_m} is the log-normally distributed random variable z for each midpoint shown in (E-8) and (E-9). It is important to note that the R_m CDF extreme was set to a value of one to conserve total probability.

$$CDF(R_{m,med}) = \frac{1}{2}\left[1 + ERF\left(\frac{Z_{R_m}}{\sigma_{\ln(R_m)}\sqrt{2}}\right)\right] \quad \text{(E-7)}$$

$$Z_{R_{m,1}} = \ln(41.67) - \ln(R_{m,med}) \quad \text{(E-8)}$$

$$Z_{R_{m,2}} = \ln(69.45) - \ln(R_{m,med}) \quad \text{(E-9)}$$

3.2.3 TC Heading

FEMA (2013) showed historic θ distributions are represented by a narrow normal curve with a mean (μ_θ) of approximately -22.5° (all angles are measured ccw from due N) and a standard deviation (σ_θ) of 10°. Resio & Irish (2015) showed the correlated variation of θ and C_p based on sampled data from the HURDAT2 records in the NYB (Figure 9), where the null hypothesis of independence was rejected even at the 0.01 level of significance. Upon sampling the current historical data with the criterion listed in Section 3.1, the statistics of TCs that have impacted the NYB resulted in a μ_θ closer to due north (N) and a much higher σ_θ (-11.61° and 30.56°, respectively) as compared to the values used in the FEMA (2013) coastal analysis.

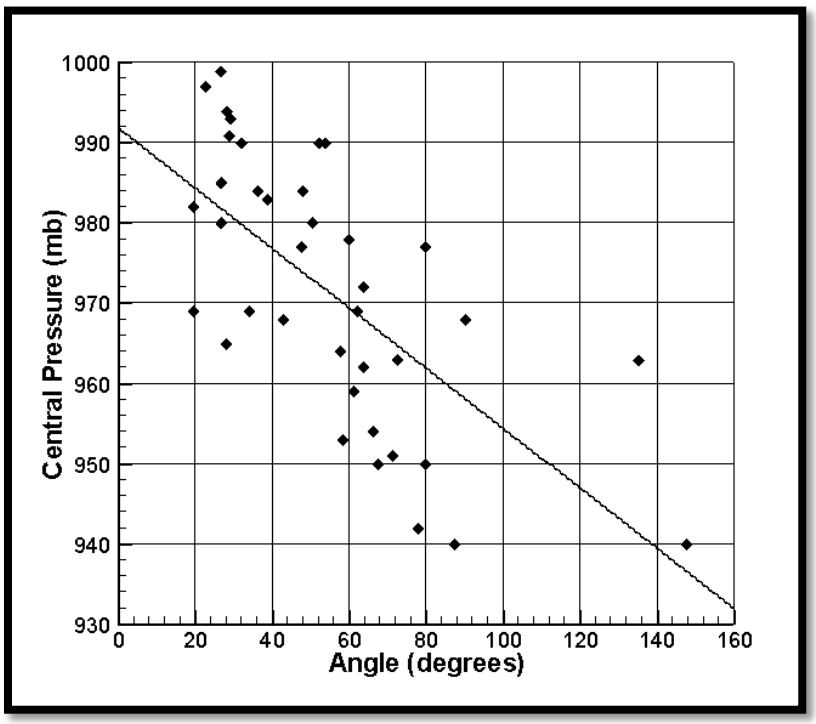

Figure 9: Variation of C_p – θ at Time of Lowest C_p (Source: Resio & Irish, 2015)

This analysis included four θ values, which encompassed the entirety of landfalling TCs in the NYB for model simulation input: (1) -22.5°, (2) 0°, (3) 22.5°, and (4) 45°. Every θ is shown in the "spaghetti" plots in Appendix B (Figures 21 and 22). Similar to the approach in the preceding section, the angle CDFs were computed using the ERFs shown in (E-10), which resulted in "angle band" PDFs for the θs selected for storm combinations. The angle band edges (θ_{edge}) were: (1) -11.25°, (2) 11.25°, (3) 33.75°, and (4) 56.25°. The CDF extreme was forced to one again here, so the remaining probability of storms higher than the 33.75° to 56.25° angle band would not be lost in the calculation.

$$CDF(\theta_{Edge}) = \frac{1}{2}\left[1 + ERF\left(\frac{Z_{\theta_{edge}}}{\sqrt{2}}\right)\right] \quad \text{(E-10)}$$

where

$$Z_{\theta_{edge}} = \frac{\theta_{edge} - \mu_{\theta}}{\sigma_{\theta}} \quad \text{(E-11)}$$

3.2.4 TC Track (Location)

Determining the set of storm tracks was completed by discretizing the landfall distribution to with an even spacing of $1R_m$ (measured perpendicularly to the track's θ). Niedoroda et al. (2010) and Toro et al. (2010a) completed sensitivity studies that showed this structure of track spacing is small enough to capture the peak surge of any event (especially when only considering one location such as Battery Park, NY). A total span of 500 km resulted in 19, 7, and 7 tracks for the 27.78, 55.56, and 83.34 km R_m values in each θ family, respectively (Figures 21 and 22 in Appendix B).

The track layout was centered near the middle of Lower Bay (73.971° W, 40.511° N) and simulated based on a straight-line approach. Storms were added to either side of the central track in the simulation process until the surge response at Battery Park, NY was less than 0.5 m. This enabled a minimization of simulations, as a surge response of this magnitude is not even the range of tides in the area. Furthermore, Resio (2007) showed that representing highly variable natural storm tracks by the approximated straight-line approach could present some error in the JPM for certain areas. However, Figure 10 shows randomly selected storm tracks from the HURDAT2 records. This plot implies that the straight-line approach may be a decent assumption for the NYB region, as the storm tracks are relatively straight upon and after landfall (excluding the anomaly – Sandy).

Figure 10: Randomly Selected Historical TCs in the NYB Region (Source: Resio, 2014)

3.2.5 TC Forward Velocity

Even though the forward speed of any storm is important, V_f has been shown by Toro (2012) to produce a scalable, consistent response and was treated parametrically with a value of 12.86 m/s. However, a study was conducted to analyze TC's surge sensitivity to this parameter in the NYB, which will be detailed later in this manuscript. Some previous investigations assumed the forward speed of TCs in this area were dependent upon the C_p of TCs in the project region and that historically more intense storms translated more quickly (FEMA, 2013). However, the sample developed for this study showed the opposite trend, with more intense storms moving somewhat slower than less intense storms. Since these two results suggest that there is uncertainty in this relationship, it was assumed here that the two parameters are independent.

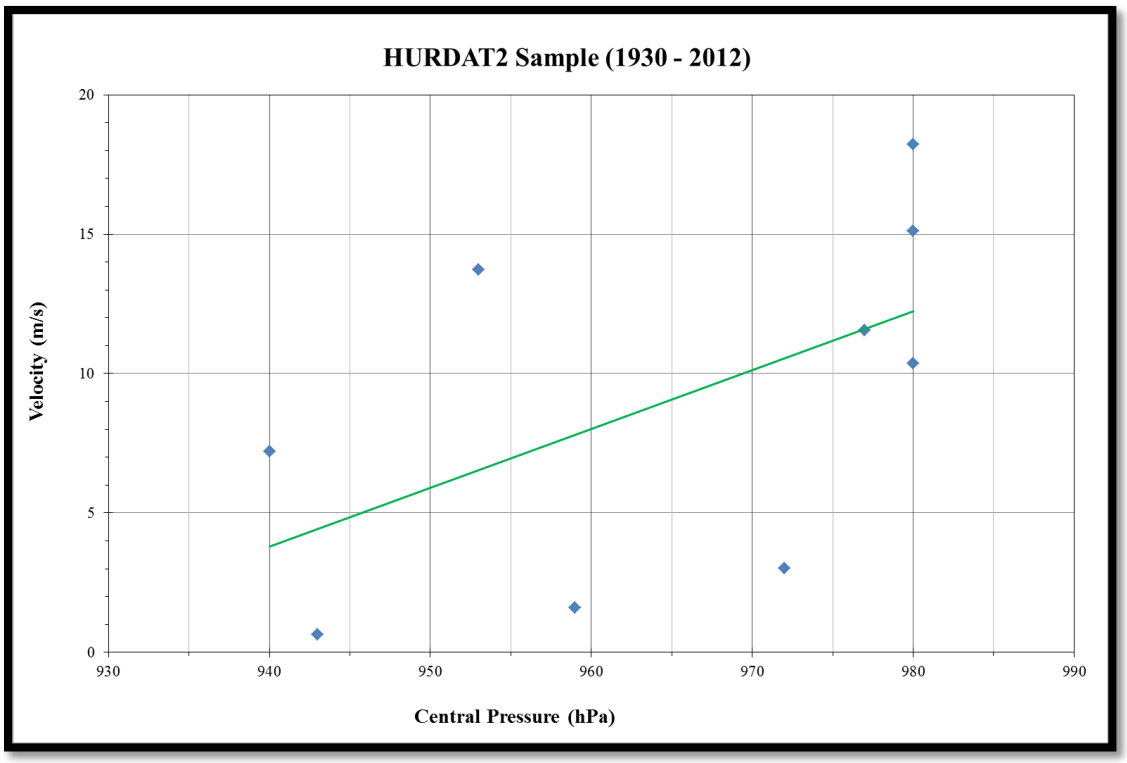

Figure 11: TC Velocity versus Central Pressure in the NYB

3.2.6 TC Pressure Profile Parameter

Holland (1980) found TCs had significant variability in the peakedness of the wind speeds along the radial distance from a TC's eye and described this variability with the dimensionless β. This parameter was described by Vickery & Wadhera (2008) to have a strong negative correlation to an increasing R_m and ψ, and a weak positive correlation to a decreasing C_p. Because that study showed β to have an average close to unity with very small variation in higher latitudes, β was included in the makeup of the synthetic storms as a constant of 1.1. The distribution parameters for β include an average of 1.1 and a standard deviation of 0.2 (FEMA, 2013).

3.3 The Surge Model: ADCIRC Simulations

The modeling process commenced when all parameter values were set and the corresponding distributions were found. The 353 synthetic storm runs were modeled using the hydrodynamic ADCIRC model (Luettich Jr. et al., 1992; Blain et al., 1994; Westerink & Luettich Jr. 1994) to represent the WSE extremes due to the time-dependent TC surge for the JPM integration (this total excluded the simulations needed for the model validation phase). The synthetic storms were divided into three simulation classes. (1) A total of 336 synthetic TCs embodied the production phase, which entailed all possible combinations of the storm characteristics. These runs were used to forecast potential WSEs in the project area, which controlled the storm surge needed for the JPM (similar to the outline in Toro et al., 2010b). (2) An additional 16 simulations were completed for the investigation of surge sensitivity due to the V_f characteristic of TCs traversing toward Battery Park, NY. (3) One final simulation was completed to omit tides from the production simulations assuming linear superposition. The tide simulation is detailed in Section 3.3.3, where the astronomical tide phase was incorporated in the AEPs by the τ term.

Figure 12 displays the resolution of the NYB's region of the grid, extending into Lower Bay and up the Hudson River valley. Improving resolution by applying smaller element sizes is essential in detailing important features in the coastal zone. It is notable that coupling hydraulic and wave models with the hydrodynamic ADCIRC model was out of the scope of this manuscript; thus, this article does not incorporate precipitation and waves in the flood frequencies described in Chapter 4. However, the importance of added water levels from precipitation and waves is recognized and could be included in future work with the surge data presented here.

The execution of the modeling process consisted of six major steps: (1) validating the ADCIRC mesh, (2) developing the wind and pressure files, (3) applying a QA/QC process for each storm's wind and pressure profiles, (4) executing each simulation on a 384-core HPC, (5) implementing a QA/QC process on the ADCIRC output, and (6) shifting the vertical datum from NAVD88 to MSL. Steps (2) through (6) were completed for all three simulation classes previously listed.

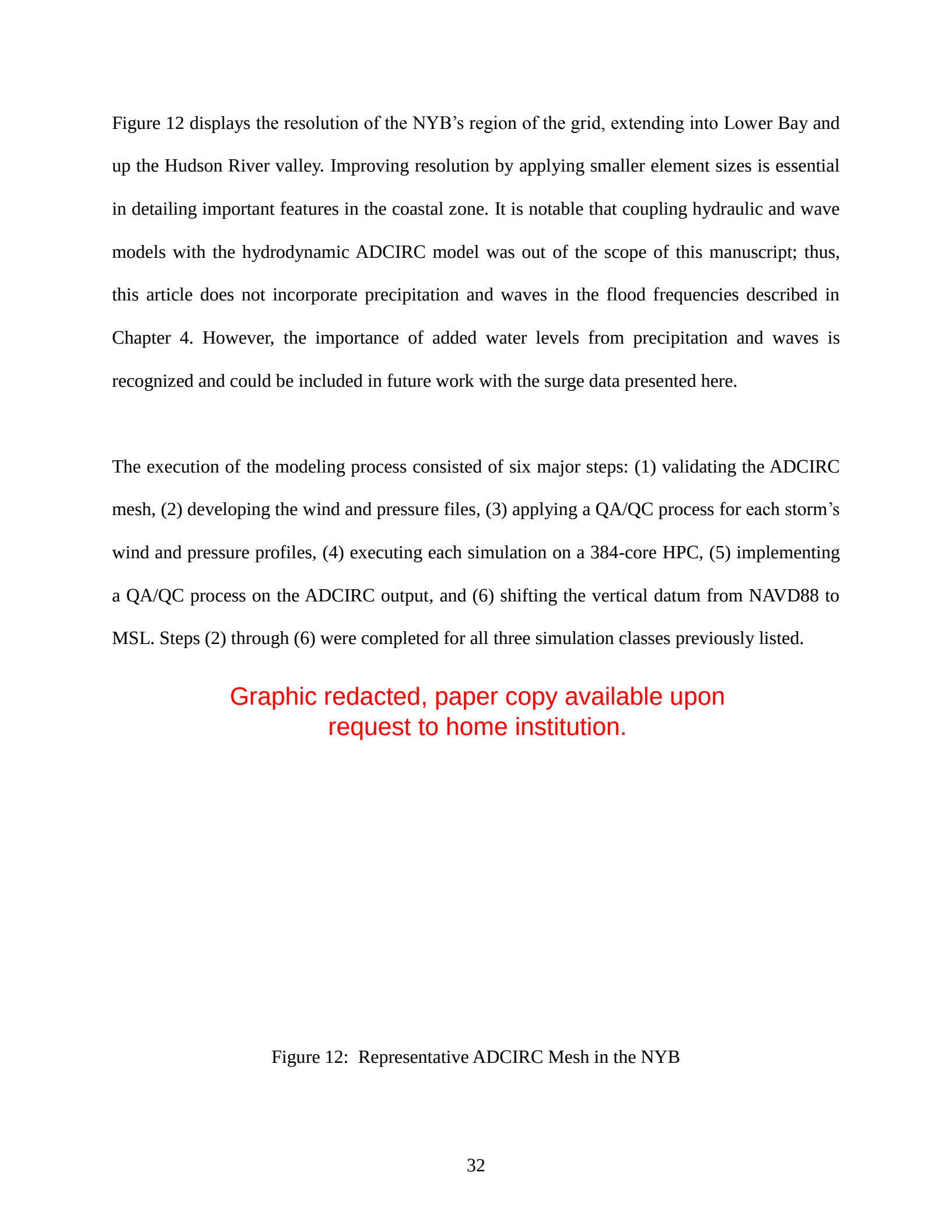

Figure 12: Representative ADCIRC Mesh in the NYB

3.3.1 Model Validation

In order for most efficient use of the HPC, two main tasks were accomplished during the validation phase: (1) verifying the output WSE of a representative storm to evaluate and validate the performance of the model's computational domain using meteorological and tidal forcings, and (2) establishing a strategic foundation for production simulations. The ADCIRC boundary control, start, wind, and pressure files (fort.15, fort.67, fort.221, and fort.222, respectively) were the only files that were changed throughout the modeling process. The attributes, river flow, and decomposition files (fort.13, fort.20, and fort.67, respectively) were not altered. The river flow component was held constant.

To make sure the provided ADCIRC mesh produced accurate WSEs for the NYB region, a synthetic storm was hindcast to imitate TC Sandy for WSE comparison (informally denoted the "benchmark simulation") for the validation phase of the modeling process. This storm was simulated on the HPC, checked for inconsistencies, and the resulting WSE levels were checked against published levels for validation of the model's grid. The WSE output from the benchmark simulation is displayed in Appendix A. Figure 17 shows how the model's solution for the benchmark simulation did not depict the surge leading up to the extreme, but it did capture the maximum WSE nicely. The output maximum WSE for the benchmark simulation was 3.276 m, and the published verified maximum WSE was 3.375 m. Because the JPM only needs extreme values for integration and the variation was only 0.1 m, the benchmark simulation validated the use of the model's grid for this study. The verified water levels can be checked with the published values on NOAA's tides and currents website.

While completing the benchmark simulation, a study was completed to address the most efficient way to simulate the hundreds of production runs that were needed for the JPM (i.e. wall clock time efficiency). Figure 18 in Appendix A shows the performance of the HPC when running multiple production storms simultaneously. One simulation utilizing all 384 processors took approximately three wall clock hours to complete, whereas eight simulations took 19 wall clock hours computing concurrently on 48 processors each. This resulted in a total of approximately five hours saved per eight storms, and a total of around nine days more efficient for all storms simulated.

The benchmark simulation utilized a 10 day spin-up time with tidal forcing and an eight day simulation time with both meteorological and tidal forcing. Because a harmonic analysis was not necessary for this study, and the time needed for the benchmark storm was only four days. This resulted in utilizing the initial 12 days from the model validation simulation as ramp time and using the modeled tide phase as the WSE for the model cold-start, which was informally noted as the "hydro-cold-start" (Figure 19). Additionally, the initial benchmark simulation consisted of the model recording WSE levels with a three minute time step. To further reduce the wall clock time needed to complete a simulation for the production phase, a six minute time step was specified in the control file for production WSE output. A total compute time of six days resulted for the production run phase of the modeling process.

3.3.2 Production Runs

The term "production" indicates the ADCIRC model was validated and ready to simulate the storms included in the JPM. This section details the production run phase and QA/QC process for each storm.

3.3.2.1 Pre-Processing Input

All synthetic events were initiated by a FORTRAN code and modeled to traverse in straight lines from southeast to northwest for $\theta > 0°$, south to north for $\theta = 0°$, and southwest to northeast for $\theta < 0°$. Every potential simulation is plotted in Appendix B (Figures 21 and 22). The white lines represent the storms that were simulated and incorporated into the JPM. The yellow lines represent the storms that were not simulated, as they either initiated over land or were thought to produce surge values below the set minimum threshold of 0.5 m (without the inclusion of tides). The process to find the yellow-lined tracks included using the straight-line approach to evaluate the magnitude of the WSE from the previously simulated storm.

A FORTRAN executable program utilized the resulting tracks to create wind and pressure fields, which were checked for completeness and relative correctness. The wind and pressure fields characterized synthetic TCs ramping up and traveling over the ADCIRC grid for a total of six days, making landfall at the 4.5 day mark. A representative production simulation is shown in Figure 20. The wetting and drying shown in this figure occurred well before landfall and did not provoke any instabilities in the surge model.

3.3.2.2 Post-Processing QA/QC

Each storm was simulated on the 384 CPU HPC, using 48 processors per storm, culminating in eight storms running in parallel. The recording station TS file (fort.61) was of importance since this study focused on Battery Park, NY and the JPM only required the surge model's extreme WSE. However, the global output files (fort.63 and maxele.63) were still checked for instabilities

in the QA/QC process. The post-processing QA/QC phase included four main checkpoints, shown in Table 4.

Table 5: QA/QC Checklist

QA/QC Checklist	
1	Did the model run to completion without large instabilities?
2	Were the prescribed output files generated (fort.61, fort.63, and maxele.63)?
3	Instabilities in fort.61 TS plots: Smooth? Outliers? Significant wetting & drying? Etc.
4	Instabilities in global maxele.63: Large gradients? Spatial anomalies? Etc.

3.3.3 Tide Simulation

One synthetic simulation was conducted to remove tidal effects from the numerical model production runs. This was done by assuming linear superposition at Battery Park, NY. This may not be a good assumption for a broad area with shallow water regions and could be a possible source of small error. However, the location of Battery Park has good coastal access (fairly open to long waves) and is relatively deep; thus, linear superposition should be an alright assumption to make. This task was accomplished by simulating a very small and weak TC (winds close to zero m/s and pressure close to typical sea level), which was essentially a simulation with no meteorological forcing, producing WSE levels only from astronomical tides.

3.3.4 Forward Velocity Sensitivity Study

The V_f parameter was considered parametrically (12.86 m/s) for all storm combinations in the production phase to minimize the number of synthetic simulations. However, the JPM still needed information on the variation of storm surge due to this characteristic. To provide this information, a sensitivity study was completed using the ADCIRC hydrodynamic model to yield

surge values separate from the JPM integration. One X (73.971° W, 40.511° N), two C_p's (960 and 920 hPa), two R_m's (27.78 and 83.34 km), two θ's (0° and 45°), and three V_f's (7.717, 12.861, and 18.006 m/s) made up the 24 TC simulations used in the sensitivity analysis of surge response due to V_f deviation. The ADCIRC WSE is shown normalized by the median value (η_*'' was the WSE of the constant V_f) in Figure 13. The 16 extra storms resulted in a scaling factor of approximately 9% that was used in conjunction with a sample mean and standard deviation of 9.048 and 6.295 m/s, respectively, in the JPM calculation. This sensitivity study allowed for a minimization in storm combinations without omitting the V_f parameter from the JPM calculation.

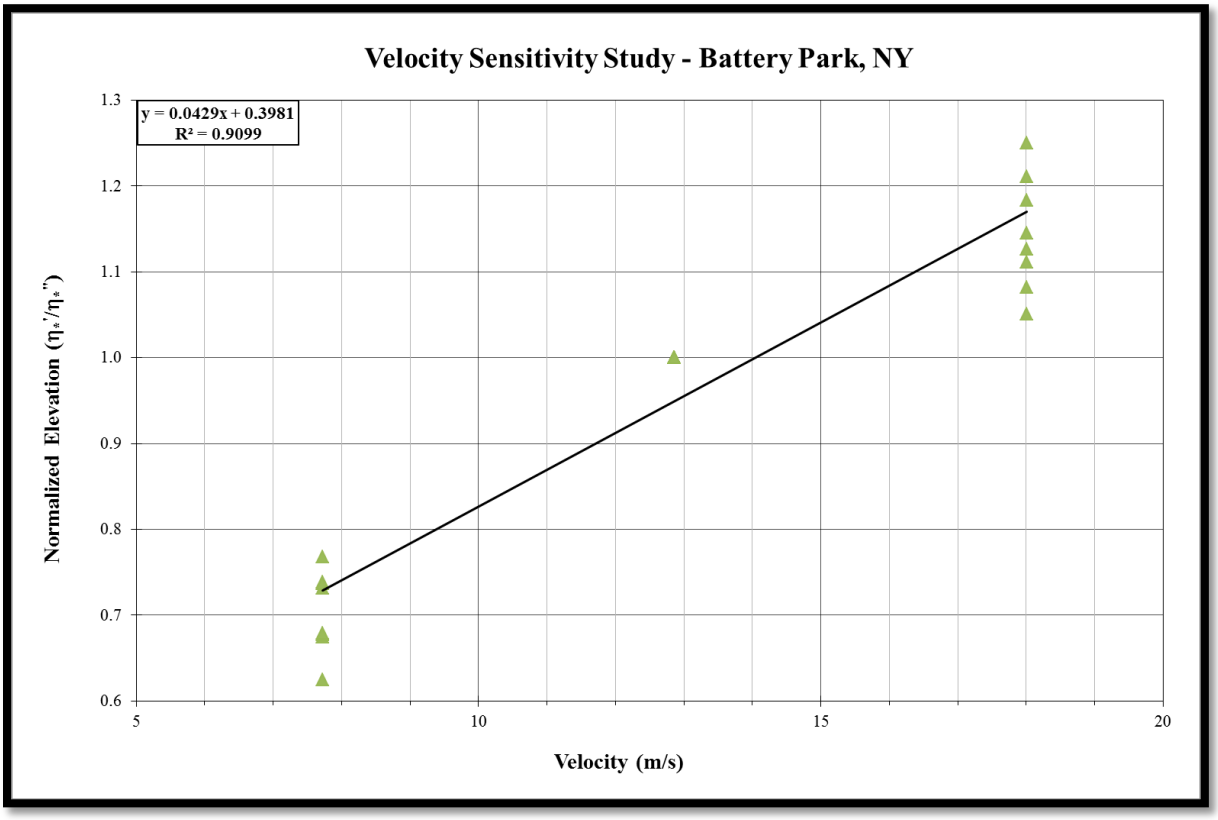

Figure 13: Normalized Velocity from ADCIRC Sensitivity Runs

Chapter 4

JPM-RS Application

The 336 production simulations produced the first RSs analyzed in the JPM-RS technique. Appendix C shows the alongshore distribution of surge levels divided into θ classes. The functional behavior of the surge response curves generally varied slowly over the span of the coastline (deviating away from the black vertical line representing the location of Battery Park, NY). Abnormal jumps in $\eta_{\#}$ can be seen on some curves, which could be attributed to numerous natural or synthetic subtleties such as a trapped wave, resonance inside Lower Bay or NY Harbor, model instabilities, etc. Some curves represented on the 45° plot shows dips in the peaks, believed to be a natural surge response during the period of TC eye landfall.

4.1 The Inclusion of Uncertainty

The final piece of information needed to calculate the AEPs resulting from the JPM was the uncertainty term (τ). Random errors with a mean equal to zero are known to increase uncertainty in TC surge predictions (Resio et al., 2015). The inclusion of these errors can be associated with epistemic or aleatory uncertainty, but appropriately accounting for them is essential to accurate flood frequencies. In this analysis, τ was used to estimate the variability due to three components of uncertainty and their impact on AEPs.

The first constituent is the astronomical tide bias due to random tide phasing and amplitude (τ_{tide}) superimposed on storm surges of variable durations. The mean tidal displacement (η_{+}) and

standard deviation (σ_{tide}) due to tides was calculated to be 0.312 m and 0.385 m, respectively (Section 4.1.1). The second contribution to uncertainty is due to errors in numerical surge model data and approximations (τ_{mod}). For example, data that is used in composing a model's grid are taken as a snapshot in time. As the earth's topographic and bathymetric features are continually changing, coastlines evolve and the data are no longer precise when simulations are subsequently executed. The standard deviation for the uncertainty due to model data and approximations ($\sigma_{\tau_{mod}}$) was taken as 0.390 m from FEMA (2013). The last component to the τ term results from the suppression of variation in complex wind fields to a simplified set of parameters (τ_s), found to have a standard deviation (σ_{τ_s}) of 0.543 m (FEMA, 2013). Because these components were assumed to be independent and approximately normal with zero mean, they were grouped together and accounted for as one term in the JPM methodology (E-13).

$$\sigma_\tau = \sqrt{\sigma_{\tau_{tide}}^2 + \sigma_{\tau_{mod}}^2 + \sigma_{\tau_s}^2} \qquad \text{(E-13)}$$

Figure 14 from Niedoroda et al. (2010) shows a representative example of the normal redistribution process taken in the JPM. Theoretically, the uncertainty term is condensed into one accumulated probability mass bin. This accumulated probability mass was symmetrically apportioned into 100 probability density bins with increments of 0.1-m, centered on the middle element. The redistribution process used the standard deviation in each bin to make up the width of the theoretically fitted normal curve (Niedoroda et al., 2010). It is important to note that the hypothetical normal redistribution in Figure 14 includes η_+, not just the components in (E-13). The reason for the discrepancy is because this study accounted for η_+ within the JPM separately, as shown by the final form (E-18) in Section 4.2.

Graphic redacted, paper copy available upon request to home institution.

Figure 14: Redistribution for Secondary Random Processes (Source: Niedoroda et al., 2010)

4.1.1 Astronomical Tides

The final component needed for the uncertainty term was the bias due to tides. This section details how tides were included in this work as uncertainty in the JPM integral. FEMA (2013) recently utilized a single random tide phase in the simulation of modeled storms. This method of incorporating tides into hazard quantification may be useful on the Gulf of Mexico's United States coastlines where tide changes are relatively small, but even FEMA (2013) noted tidal fluctuations in the NYB can range from 1.07 – 2.44 m, with a possible maximum range of up to 3.35 m. Irish et al. (2011) showed this magnitude of variation could introduce sampling errors and should be considered separately.

Since Battery Park is not located far up the Hudson River and the water is relatively deep, the combination of tides and water levels were assumed to be adequately approximated by linear superposition. Therefore, the expected WSE extreme from TC surge and tides was represented by (E-14).

$$\eta_{total} = \eta_{srg} + \eta_{tide} \quad \text{(E-14)}$$

The predicted astronomic tide signal was retrieved from the NOAA tides and currents website (Station 8518750). The station data were read in to a FORTRAN code that allowed the synthetic surge TS values to step through the tide cycle an hour at a time. This permitted each storm to impact Battery Park at any time (on an hourly basis) over a 14-day tidal signal, ranging from May 28th, 2012 to June 11th, 2012 to capture the largest tide range of the year (maximum station WSE was 1.004 m). Because one anomalistic month is approximately 27.554 days, a two week period was sufficient to incorporate neap and spring semidiurnal tides for the extreme value analysis. The surge TS was represented by a normal distribution, shown mathematically in (E-15).

$$\eta(t) = \eta_{th,max} e^{\left[-(t-t_{peak})/2\sigma_s^2\right]} \quad \text{(E-15)}$$

where

- $\eta_{th,max}$ is the theoretical maximum surge (m),
- t_{peak} is the time of maximum theoretical surge (hours), and
- σ_s is the average half-surge duration (hours).

To implement the normal curve for any surge value at any time over the tidal cycle, a standard deviation needed to be estimated for the width of the surge normal distribution. Because the JPM evaluates extremes, the average standard surge duration was estimated by (E-16).

$$\frac{\eta(t)}{\eta_{th,max}} = e^{[-(\hat{t}-\mu_s)/2\hat{\sigma}^2]} = 0.5 \quad \text{(E-16)}$$

where

- $\hat{t}$ is the time to go from the peak of the normal curve to the 50% threshold (hours),
- μ_s is the mean surge duration, taken to be zero (hours), and
- $\hat{\sigma}$ is the average surge standard deviation (hours).

(E-17) was accomplished by taking the natural logarithm of both sides and solving for $\hat{\sigma}$.

$$\hat{\sigma} = \frac{\hat{t}}{1.1774} \quad \text{(E-17)}$$

The value of 1.1774 converts the standard deviation to the length of time to go from the peak of the normal curve to the 50% threshold. Because $\hat{t}$ is the time to go from the peak on the normal curve to the halfway point on one side, (E-18) represents the surge duration needed for (E-15).

$$\sigma_s = \frac{t_{srg}}{2.3548} \quad \text{(E-18)}$$

where

- t_{srg} is the average surge duration from the production simulations, found to be approximately 12 hours.

This resulted in an average half-surge duration (σ_s) of 5.096 hours, which was implemented into (E-15). Allowing theoretical surge normal distributions with maximum values of one to eight m to step through the entire 14-day tidal cycle yielded Table 7. This table shows the resulting tide bias (η_+) and standard deviation (σ_{tide}) included in the τ term which culminated from the FORTRAN code. Table 7 also shows how the tide bias affects smaller storms more so than larger storms. Constant values of 0.249 m and 0.385 were used for the η_+ and σ_{tide} values for the JPM calculation, respectively, as they were associated with the surge value that was projected to be around the 100-year storm threshold.

Table 6: Mean Tidal Displacement & Tide Uncertainty at Battery Park, NY

Theoretical Surge (η_{th})	**Mean Tidal Displacement (η_+)**	**Standard Deviation (σ_{tide})**
m	**m**	**m**
1	0.498	0.207
2	0.354	0.304
3	0.249	0.385
4	0.173	0.444
5	0.118	0.482
6	0.079	0.506
7	0.051	0.522
8	0.030	0.532

4.2 Visualizing the JPM-RS

JPM integration commenced when the probability distributions for all required storm characteristics, the synthetic storm surge results, and the uncertainty contributions were all determined. (E-19) displays the final form of the JPM and shows how the JPM space can have as many dimensions (parameters) necessary to characterize a particular storm. This equation also

mathematically portrays the JPM's ability to interpolate at any intermediate point on the surface response created by the combination of the surge response (elevation of the synthetically driven storm) and the joint probability distributions of the parameters.

$$F\left(\eta_{max} > \eta\right) = \lambda \int \ldots \int P\left(C_p, R_m, \theta, \mathrm{X}, V_f\right) P\left(\eta_{\#} + \tau + \eta_{+} > \eta\right) dC_p dR_m d\theta d\mathrm{X} dV_f d\tau d\,\eta_{+} \quad \text{(E-19)}$$

To help understand the JPM-RS visually, Cialone et al. (2008) graphically represented a three-dimensional example of the five-dimensional JPM space, where a portion of Figure 15 was borrowed from that work. Figure 15 shows two matrices, where a set of X's and V_f's with distinct values of R_m (where $R_m \approx R_p$), C_p, and θ are displayed on top of each other. The top matrix is theoretically considered the surge matrix, where each small box represents a single synthetic storm simulated with those characteristics by the ADCIRC hydrodynamic model (highlighted in yellow and denoted $\eta_{\#}$). The bottom matrix is theoretically considered the probability matrix, where each small box represents the joint probability of the associated characteristics that make up that storm (highlighted in yellow and denoted P(η_*)). The point of showing the two matrices on top of one another is to show they share a common reference, where the resulting combination yields response surfaces within the box defined by the parameters listed in (E-19). The interesting aspect of the RS technique is that the setup allows for interpolation (in five dimensions) in boxes and in between boxes, where a 0.1-m interpolation increment was utilized in this analysis. It is important to note that since the V_f parameter treated parametrically with a 9% scaling function, the middle V_f (highlighted in green) represents the constant value held for each production simulation and the boxes on top and bottom represent the scaled values.

Graphic redacted, paper copy available upon request to home institution.

Figure 15: 3-D Portrayal of the 5-D JPM-RS Discretized Space (Original: Cialone et al., 2008)

Chapter 5

TC Surge Probabilities Using the JPM-RS

After all the necessary steps detailed in Section 2.1 were fulfilled to complete the JPM calculation, the probability curves were developed and analyzed. This chapter details the resulting curves with a discussion on how different assumptions inherent in the process could impact the projected frequencies for the NYB.

5.1 Heading Probability Discussion

The previously discussed plots in Appendix C may also support Figure 9 (Section 3.2.3) and Table 7 (this section), as it appears from the plots that surge response magnitude diminished as storm headings rotated clockwise from the 45° heading class. Table 7 shows the θ probabilities using the distribution parameters from FEMA (2013) compared compared to the θ probabilities using the distribution parameters found in this study. The θ probability in the last angle band is particularly important, as TC Sandy impacted the study region in this angle band. Therefore, having no probability within the last angle band is unrealistic if considering all possible storms within the JPM storm set. Later in this chapter, this discrepancy is shown to make a difference in the resulting flood frequencies at Battery Park, NY. It is notable that because the θ parameter was found to have an approximately normal distribution with finite tails, any probability mass at the distribution extreme was designated to the end angle band.

Table 7: TC Heading Probabilities Using FEMA Region II Statistics

Heading*	**Angle Band (From Midpoint)**		**Distribution Parameters from Storms Sampled in this Analysis**		**Distribution Parameters from FEMA (2013)**	
			μ_θ	σ_θ	μ_θ	σ_θ
			-11.611°	**30.560°**	**-22.500°**	**10.000°**
			Probability			
-22.5°	-∞	-11.25°	0.5047		0.8697	
0.0°	-11.25°	11.25°	0.2681		0.1299	
22.5°	11.25°	33.75°	0.1583		0.0004	
45.0°	33.75°	56.25°	0.0689		0.0000	

*All angles were measured ccw from due north.

5.2 Return Period for Battery Park, NY

The resulting JPM-RS return period plot for Battery Park, NY is shown in Figure 16, where the return period was simply found by (E-20).

$$T_\eta = \frac{1}{\left[1-F\left(\eta_{max,(1-yr)}\right)\right]} \quad \text{(E-20)}$$

Figure 16 shows the comparison of extreme WSE return periods using this manuscript's assumptions (solid and dashed blue lines) versus using the assumptions outlined in FEMA (2013) (solid and dashed green lines). The 100-year total WSE using this work's assumptions versus the results using the FEMA (2013) assumptions was approximately 3.0 and 2.1 m, respectively, leading to a variation of around 0.9 m. This discrepancy is mainly based on assuming statistical independence between θ and C_p, which can inherently lead to misestimated distribution parameters (Figure 9 and Table 6). Figure 16 shows that the consequences of this assumption could be underestimating TC surge probabilities in the NYB.

Figure 16 also shows the relative importance of the τ term, as it was found to be approximately 0.4 and 0.7 m at the 100-year level using the assumptions in this study versus using the assumptions in FEMA (2013) at the 100-year level, respectively. These values come from a combination of the uncertainty bias introduced into the maximum values during TC surge and the randomness around the bias (Table 7).

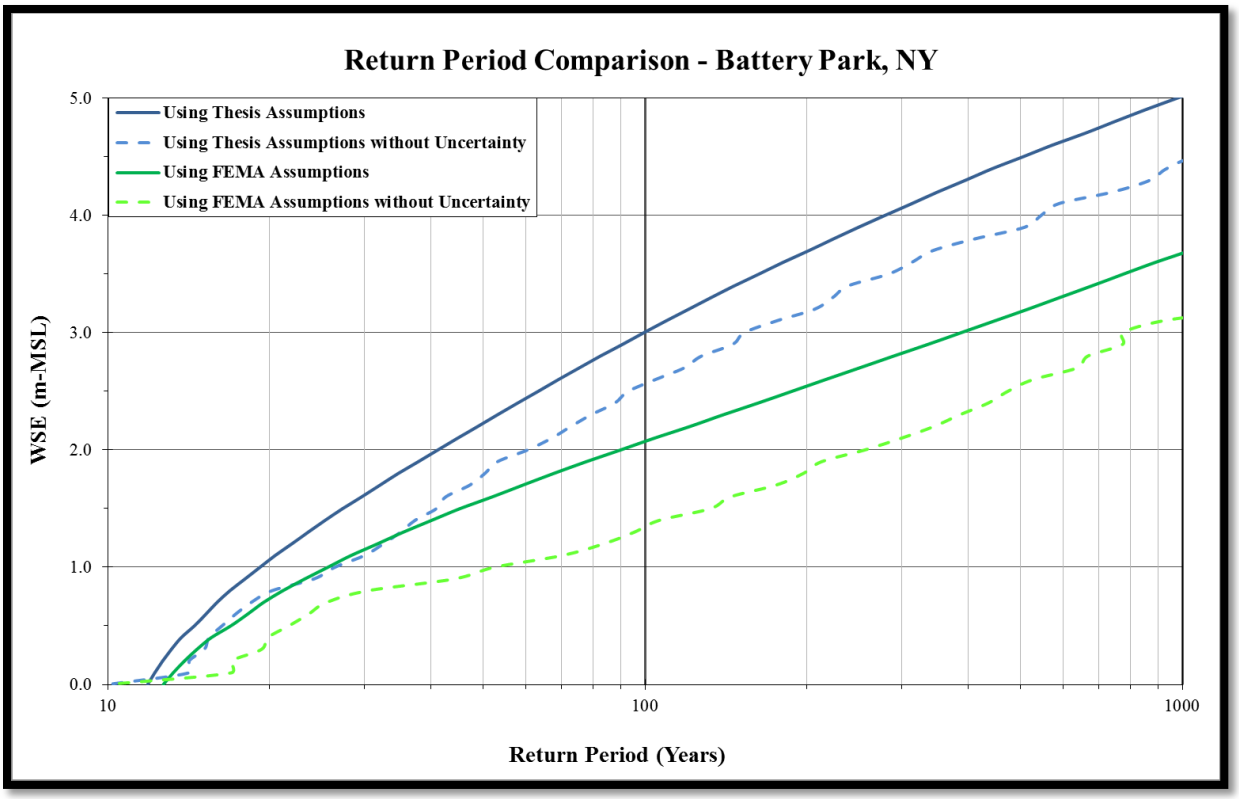

Figure 16: Return Period for Battery Park, NY

Chapter 6

Discussion & Conclusions

Quantifying the potential for natural coastal hazards and knowing how to properly mitigate the potential danger posed by such events is essential for long-term sustainability in coastal regions. This manuscript has presented the information and steps necessary to quantify surge frequencies due to TCs in the NYB. This analysis applied the JPM-RS technique, bypassing OS by utilizing 336 production ADCIRC simulations. However, the synthetic dataset is unimportant if the local climatology is not represented accurately, as misinterpreting the local climatology with unrealistic assumptions could lead to misestimating TC surge inundation frequencies.

Even with technological advancements and much improved processes that project potential flood frequencies, studies like this can still be improved upon. Drawbacks such as sparse historical data due to naturally sporadic TC events and localized WSE extremes lead to small sample sizes, limiting how far out a scientist can project the AEPs that result from the JPM. For example, the sample in this study only incorporated nine storms over 83 years. This would mean projecting probabilities past the 100-year flood event may lead to misestimating probabilities due to extrapolation. Drawbacks are also prevalent within the modeling process. Even though this manuscript detailed the hundreds of simulations executed with a hydrodynamic model, surge is not the only component to hazards such as TCs. Coupling hydraulic and wave models with the hydrodynamic dataset formed here could better encompass the flood WSEs from a natural TC due to the effects of precipitation and waves, respectively. Furthermore, incorporating the

variability of TCs could be insignificant in relation to the potential impacts that long-term processes such as sea level trends could have on vulnerable shorelines such as the NYB. As Resio et al. (2015) noted, general sea level forecasts show sea level trending upward and vary by an order of magnitude, which could possibly result in a positive bias in base flood level projections not accounted for in this study. Even though this work developed a detailed estimate of TC surge hazards in the NYB with a look into the impact of different assumptions inherent in the JPM process, the preceding limitations in this study provide a basis for future work.

Appendix A

THE ADCIRC MODEL – VALIDATION & HPC EFFICIENCY

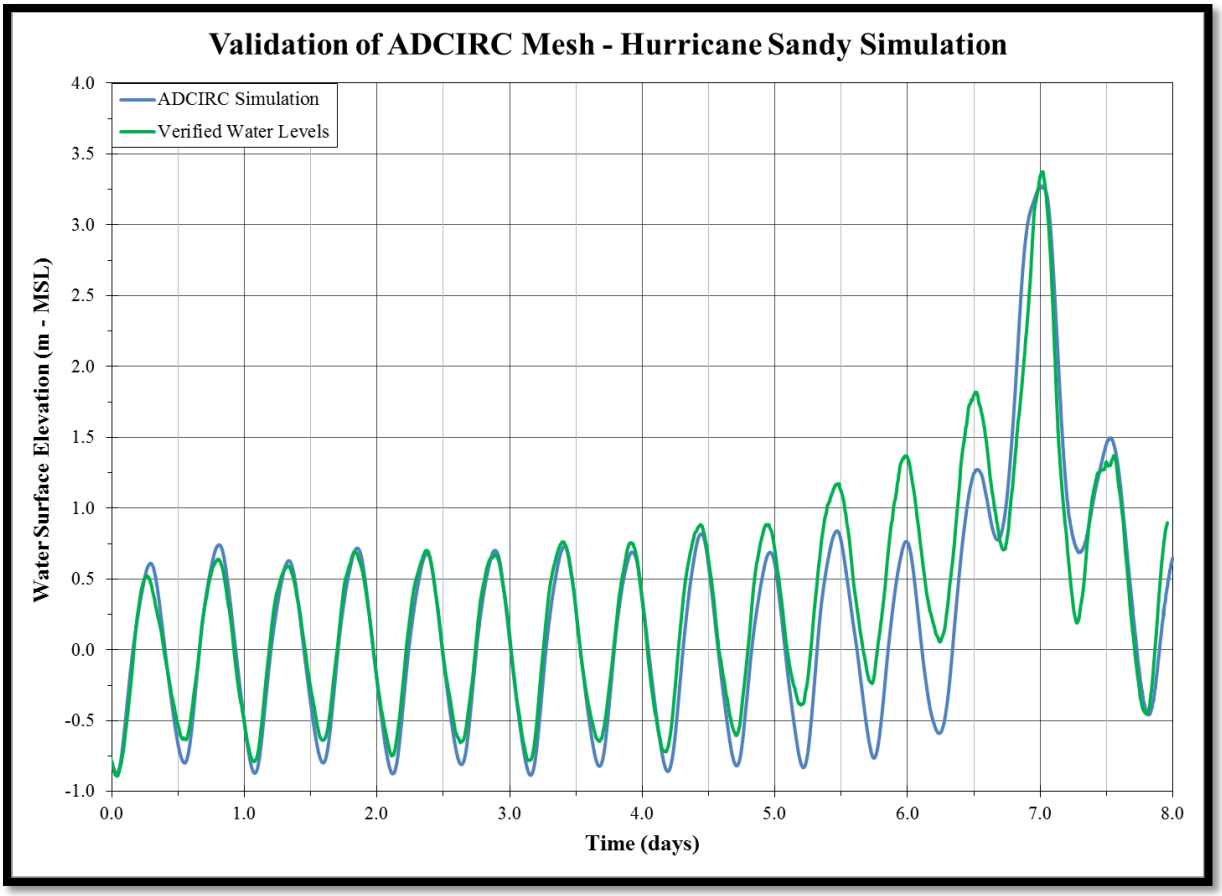

Figure 17: ADCIRC Mesh Validation at Battery Park, NY (TC Sandy Conditions)

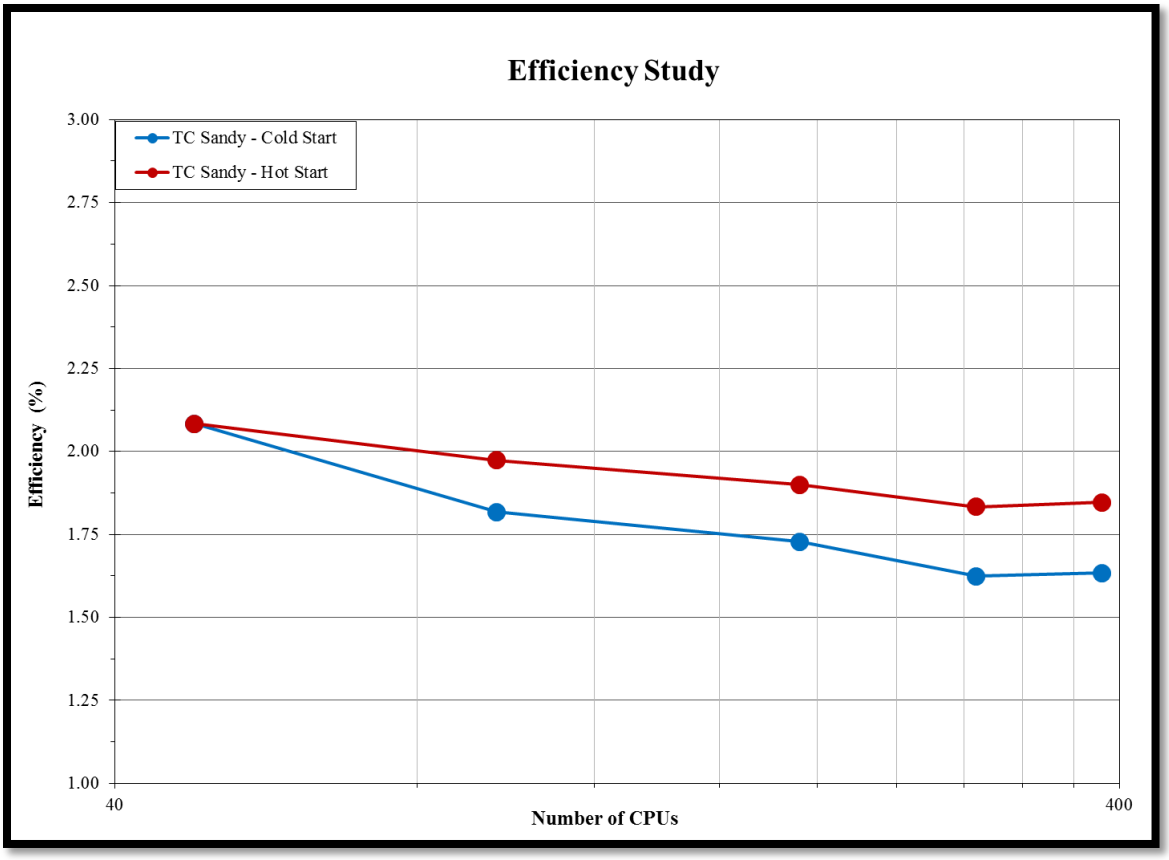

Figure 18: HPC Efficiency Study for the Determination of How Many Processors to Run On

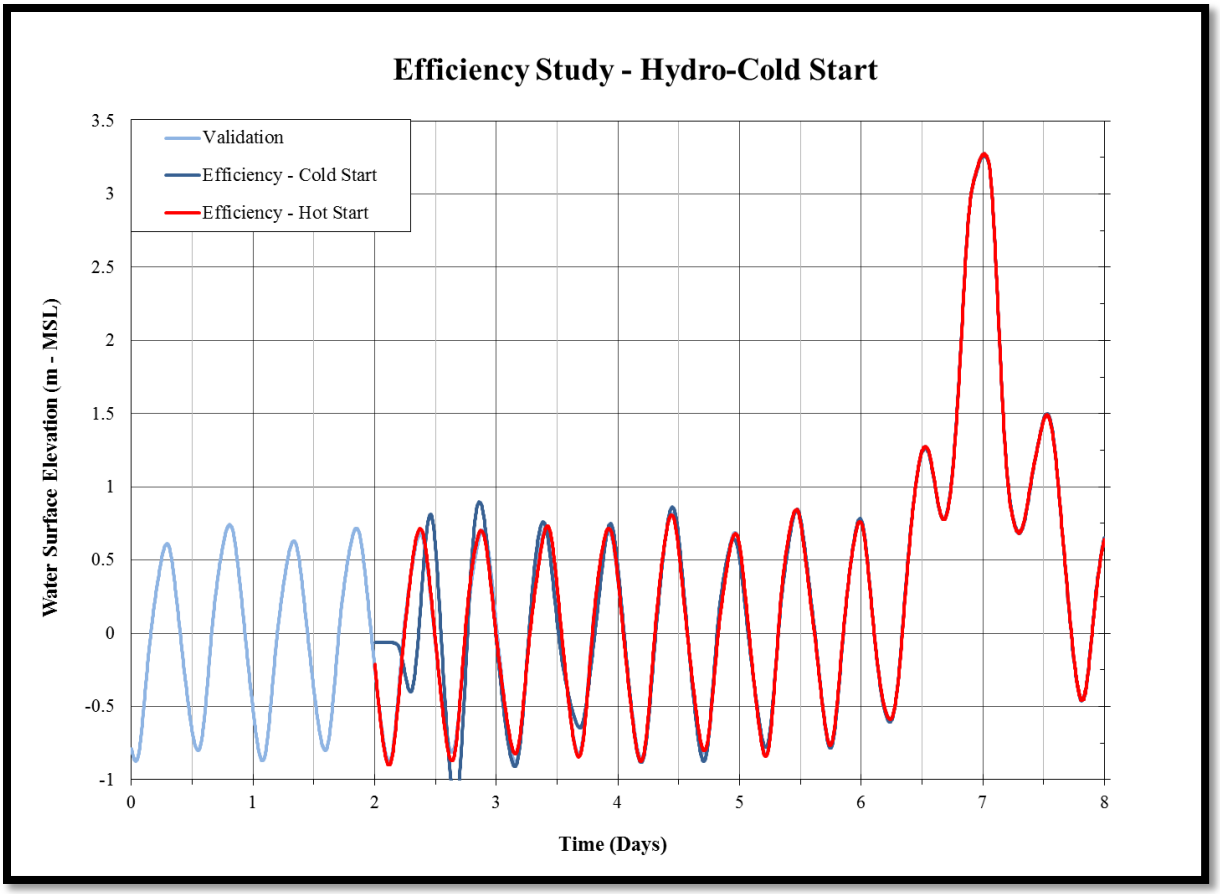

Figure 19: HPC Efficiency Study for the Determination of a Cold- or Hot-Start

Appendix B

THE ADCIRC MODEL – PRODUCTION SIMULATIONS & TC TRACKS

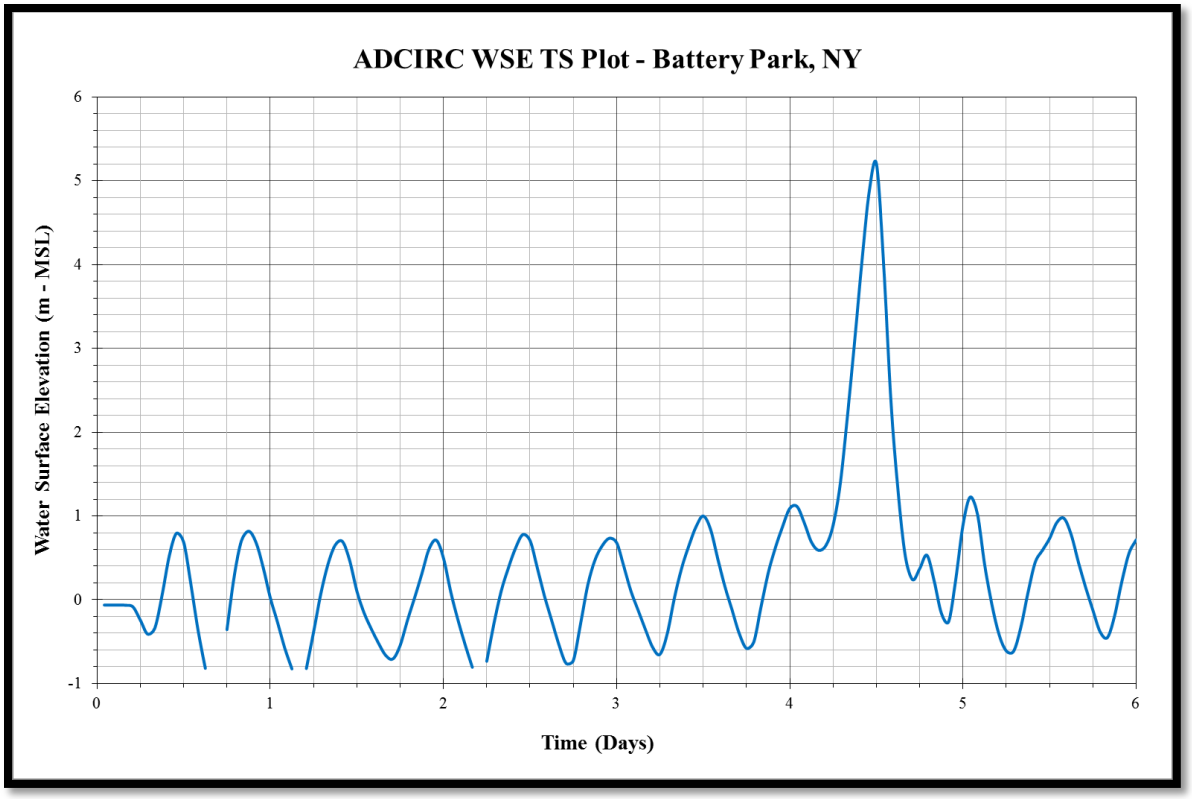

Figure 20: Representative TS Plot of Randomly Selected Synthetic Production Simulation

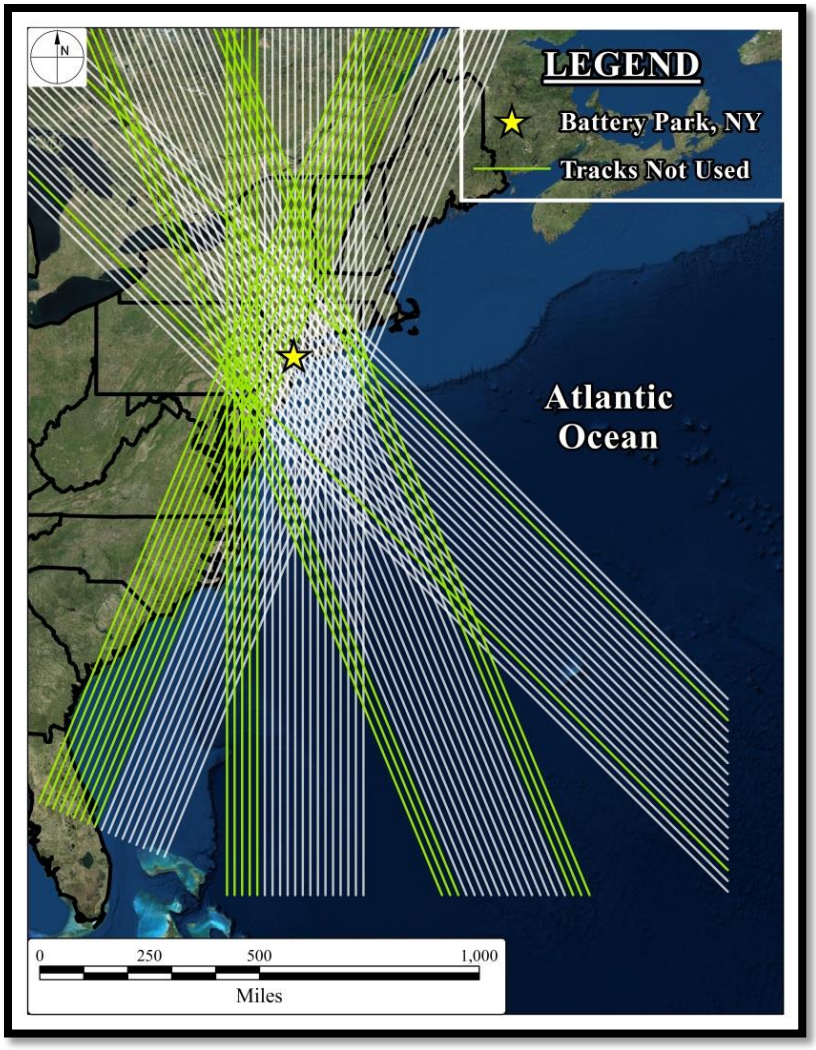

Figure 21: Spaghetti Plot of Simulated Storm Tracks for Production Simulations

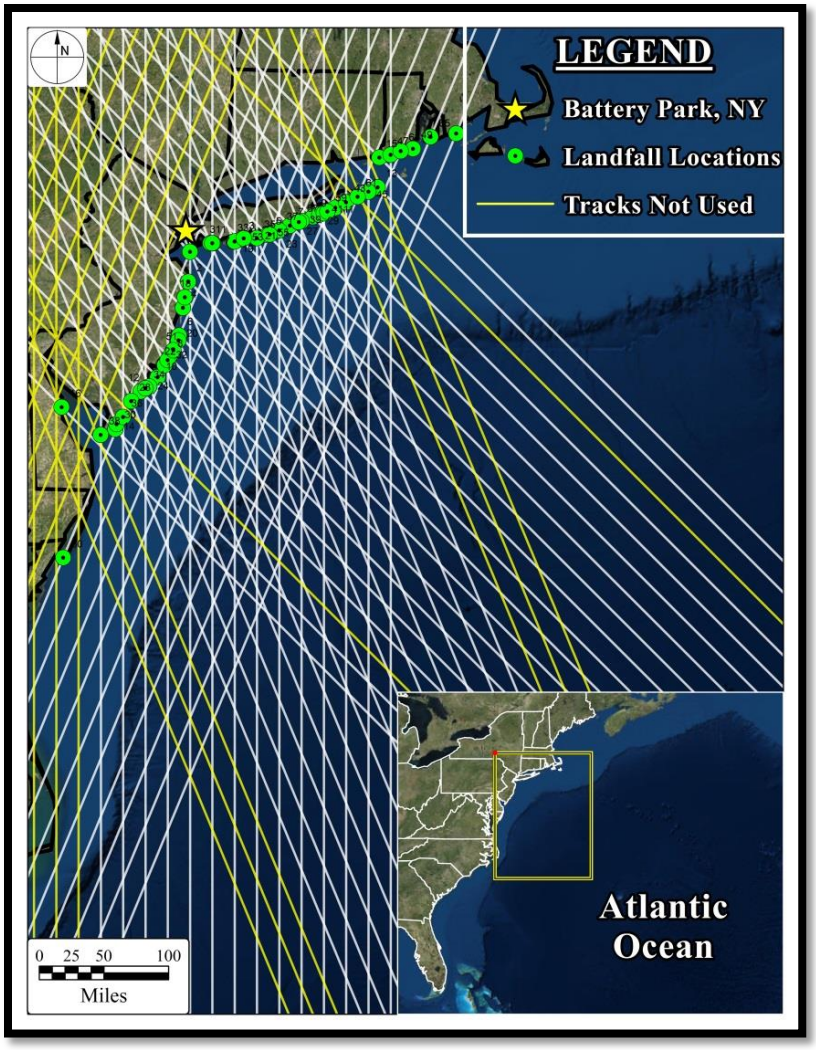

Figure 22: Landfall Locations in the NYB from Synthetic Production Simulations

Appendix C

Surge Response Surfaces

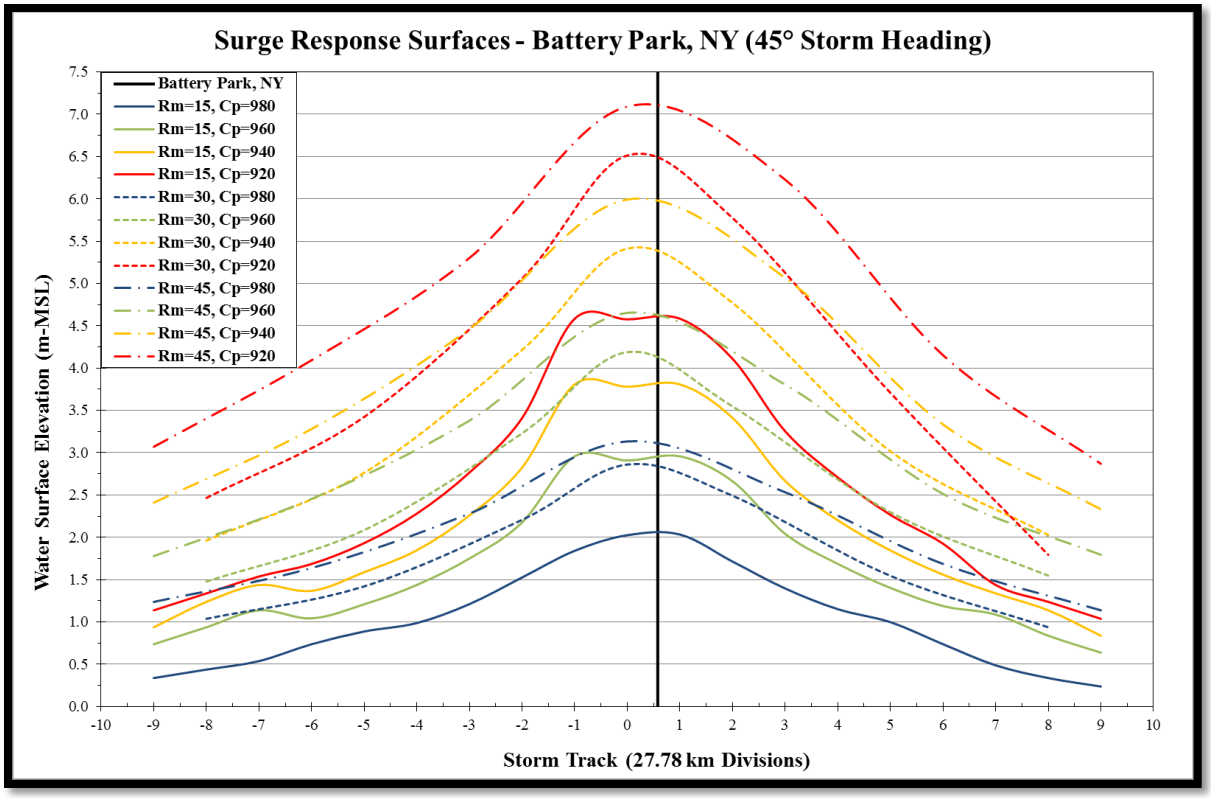

Figure 23: Alongshore Model Surge Distribution in the NYB (45° Storm Heading)

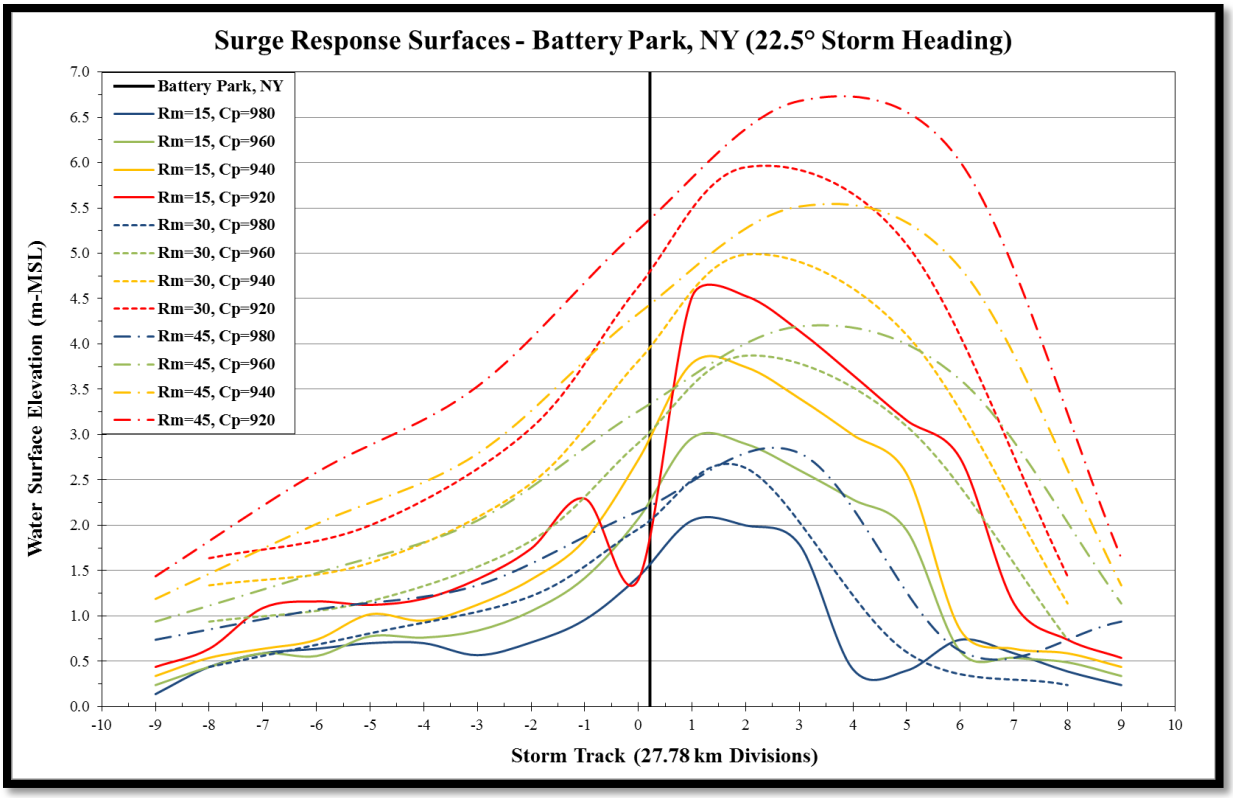

Figure 24: Alongshore Model Surge Distribution in the NYB (22.5° Storm Heading)

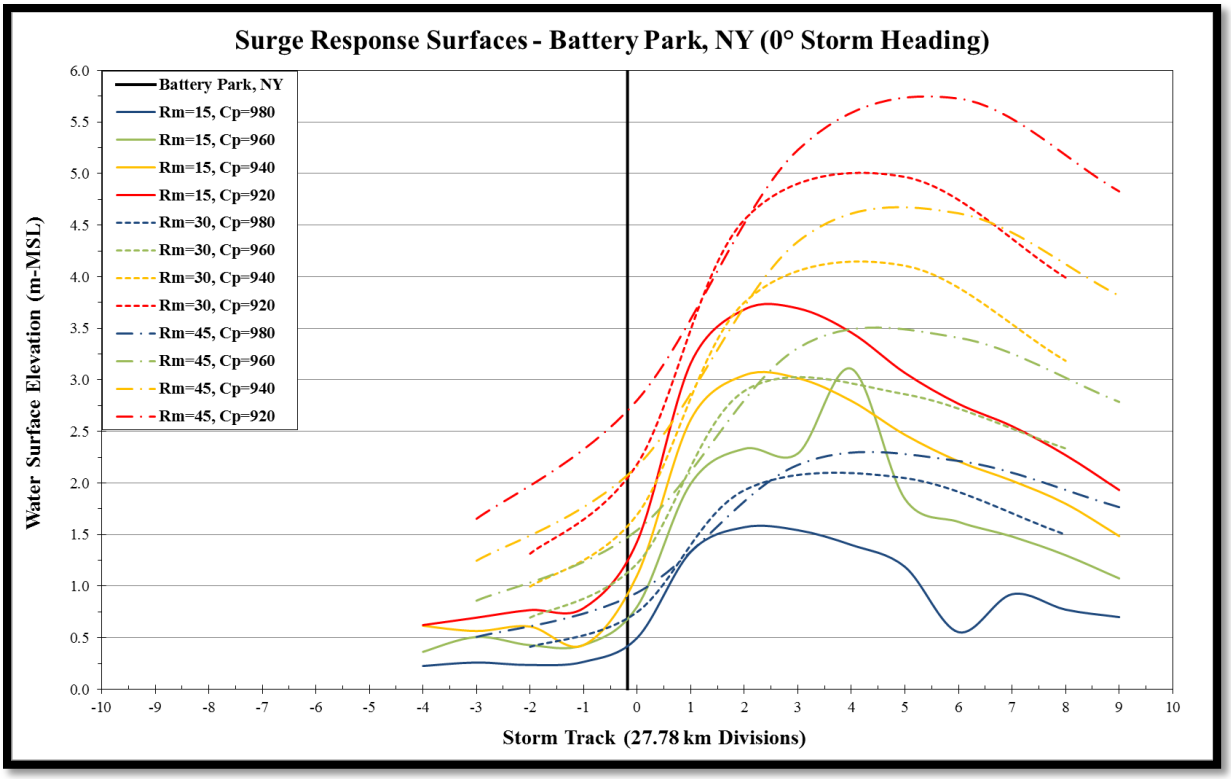

Figure 25: Alongshore Model Surge Distribution in the NYB (0° Storm Heading)

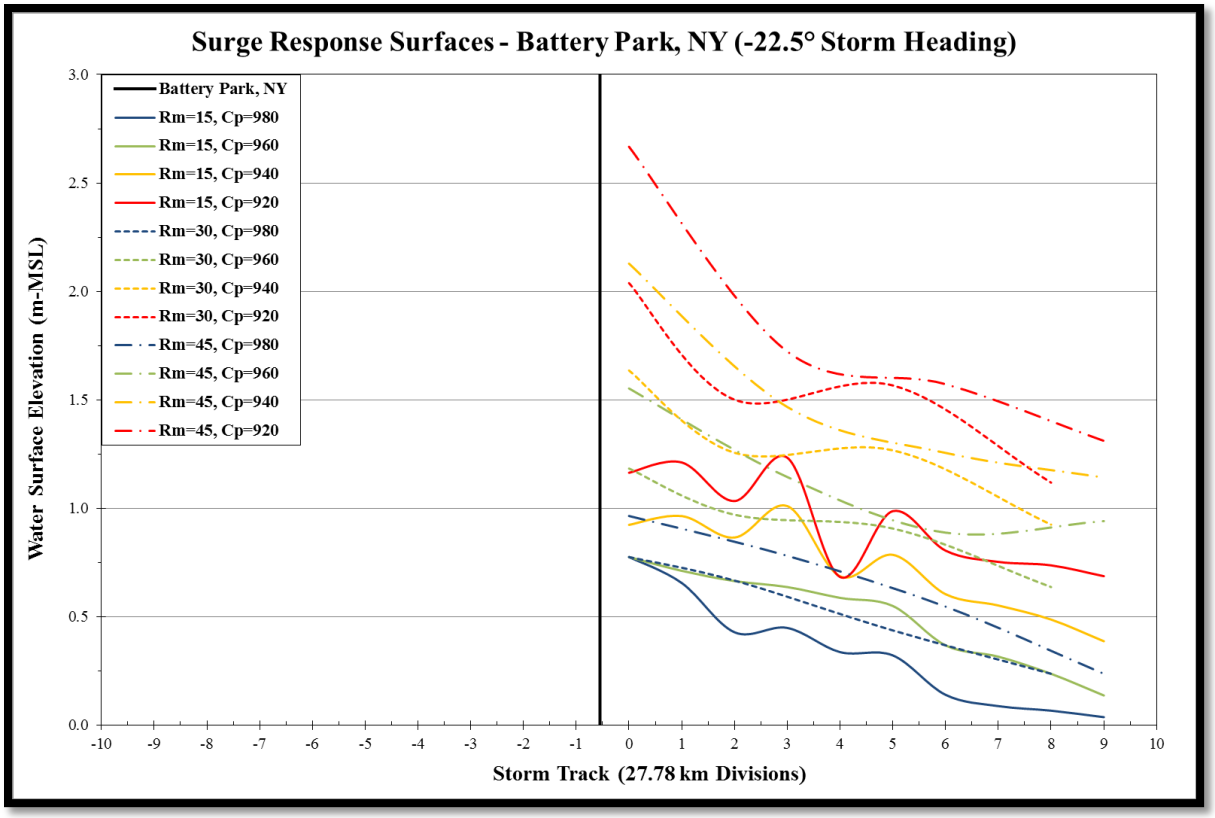

Figure 26: Alongshore Model Surge Distribution in the NYB (-22.5° Storm Heading)

REFERENCES

(ADCIRC, 2015)
Advanced Circulation (ADCIRC). Hydrodynamic model unit files and parameter definitions reference website. Retrieved 2015. Retrieved from from http://adcirc.org/

(Aberson et al., 2006)
Aberson, S. D. et al., (2006). Thirty years of tropical cyclone research with the NOAA P-3 aircraft. *Bull. Amer. Meteor. Soc.* Vol. 87, Iss. 8, pp. 1039 – 1055.

(Beven & Kimberlain, 2014)
Beven II, J. L., Kimberlain, T. B., (2014). Tropical cyclone report: Hurricane Gustav. National Oceanic & Atmospheric Administration: National Hurricane Center. Original copy 2009, revised 2014.

(Blain et al., 1994)
Blain, C. A. et al., (1994). ADCIRC: An advanced three-dimensional circulation model for shelves, coasts, & estuaries. Report 4 – Hurricane storm surge modeling using large domains. *Dredging Research Program*. Technical Report DRP-92-6. 55 pp.

(Cialone, et al., 2008)
Cialone, M. A. et al., (2008). Mississippi coastal improvement program (MSCIP): Statistical evaluation of lines of defense. *Proceedings of the 31st International Conference on Coastal Engineering.* Hamburg, Germany.

(Chouinard & Liu, 1997)
Chouinard, L. M., Liu, C., (1997). Model for recurrence rate of hurricanes in Gulf of Mexico. *J. Water., Port, Cst., Ocean Eng.* Vol. 123, Iss. 3, pp. 113 – 119.

(Collins & Viehmann, 1971)
Collins, J. I., Viehmann, M. J., (1971). A simplified model for hurricane wind fields. Paper 1346. Proceedings from the Offshore Technology Conference, Houston, TX.

(Dean & Dalrymple, 1991)
Dean, R. G., Dalrymple, R. A., (1991). Water wave mechanics for engineers and scientists. Singapore. World Scientific Press.

(Dean & Dalrymple, 2002)
Dean, R. G., Dalrymple, R. A., (2002). Coastal Processes with engineering applications. Cambridge, United Kingdom. Cambridge University Press. 1st Ed., pp. 79 – 336.

(Diaconis, 1998)
Diaconis, P., (1998). Bayesian numerical analysis. *Stat. Decision Theory & Relat. Top. IV*, Vol. 1, pp. 163 – 165.

(Divoky & Resio, 2007)
Divoky, D., Resio, D. T., (2007). Performance of the JPM and EST methods in storm surge studies. Proceedings from the 10th International Workshop on Wave Hindcasting & Forecasting & Coastal Hazard Assessment, Session K. Oahu, Hawaii. Retrieved from http://www.waveworkshop.org/10thWaves/ProgramFrameset.htm

(Dvorak, 1975)
Dvorak, V. F., (1975). Tropical cyclone intensity analysis & forecasting from satellite imagery. *Mon. Wea. Rev.*, Vol. 103, Iss. 5, pp. 420 – 462.

(Dvorak, 1984)
Dvorak, V. F., (1984). Tropical cyclone intensity analysis using satellite data. *NOAA Tech. Rpt.* NESDIS No. 11, 47 pp.

(Dvorak, 1995)
Dvorak, V. F., (1995). Tropical clouds & cloud systems observed in satellite imagery. *Trop. Cycl.*: Workbook Vol. 2, NOAA/NESDIS.

(FEMA, 2013)
Federal Emergency Management Agency, (2013). Joint probability analysis of hurricane flood hazards for New York – New Jersey. *RAMMP Joint Venture*. Draft Report (Rev. 2)

(FEMA, 2014)
Federal Emergency Management Agency, (2014). Flood Insurance Rate Map (FIRM). *Flood-plain Management*. Retrieved from https://www.fema.gov/floodplain-management/flood-insurance-rate-map-firm#0

(Google Earth, 2015)
Google Earth, 2015. Screen shots from Google Earth Pro.

(Hagen et al., 2012)
Hagen, A. B., et al., (2012). A reanalysis of the 1944 – 53 Atlantic hurricane seasons – The first decade of aircraft reconnaissance. *J. Clim.*, Vol. 25, Iss. 13, pp. 4441 – 4460.

(Ho & Myers, 1975)
Ho, F. P., Myers, V. A., (1975). Joint probability method of tide frequency analysis applied to Apalachicola Bay and St. George Sound, Florida. *NOAA Tech. Rpt.* Vol. 18.

(Holland, 1980)
Holland, G. J., (1980). An analytic model of the wind and pressure profiles in hurricanes. *Mon. Weather. Rev.*, Vol. 108, Iss. 8, pp. 1212 – 1218.

(Irish et al., 2008)
Irish, J. L. et al., (2008). The influence of storm size on hurricane surge. *J. Phys. Oceanogr.*, Vol. 38, Iss. 9, pp. 2003 – 2013.

(Irish et al., 2009)
Irish, J. L. et al., (2009). A surge response function approach to coastal hazard assessment. Part 2: Quantification of spatial attributes of response functions. *J. Nat. Haz.*, Vol. 51, Iss. 1, pp. 183 – 205.

(Irish & Resio, 2010)
Irish, J. L., Resio, D. T., (2010). A hydrodynamics-based surge scale for hurricanes. *J. Ocean Engr.*, Vol. 37, Iss. 1, pp. 69 – 81.

(Irish et al., 2011)
Irish, J. L. et al., (2011). Statistical properties of hurricane surge along a coast. *J. Geophys. Res.* Vol. 116, Iss. C10, 15 pp.

(Jarvinen et al., 1984)
Jarvinen, B. R. et al., (1984). A tropical cyclone data tape for the North Atlantic Basin, 1886 – 1983: Contents, limitations, & uses. *NOAA Tech. Memo. NWS NHC 22*. 21 pp.

(Kantha, 2012)
Kantha, L., (2012). Classification of hurricanes, typhoons, & cyclones. Chapter 9 of *Eddies & Hurricanes: Formation, triggers, & impact*. Tarasov, A. & Demidov, M. (Eds.) NOVA Science Publishers, 10 pp.

(Kay, 2014)
Kay, S., (2014). Factors affecting storm characteristics in The Battery and vicinity. Unpublished thesis, University of North Florida.

(Landsea et al., 2004a)
Landsea, C. W. et al., (2004). The Atlantic hurricane database re-analysis project: Documentation for the 1851 – 1910 alterations & additions to the HURDAT database. *Hurricanes & typhoons: Past, present, & future*. Murnane, R. J., Liu, K. (Eds.). New York City, New York. Columbia University Press. Pp. 177 – 221.

(Landsea et al., 2004b)
Landsea, C. W. et al., (2004). A re-analysis of Hurricane Andrew's intensity. *Bull. Amer. Meteor. Soc.*, Vol. 85, Iss. 11, pp. 1699 – 1712.

(Landsea et al., 2008)
Landsea, C. W. et al., (2008). A re-analysis of the 1911 – 20 Atlantic hurricane database. *J. Clim.*, Vol. 21, pp. 2138 – 2168.

(Landsea et al., 2012)
Landsea, C. W. et al., (2012). A re-analysis of the 1921 – 30 Atlantic hurricane database. *J. Clim.*, Vol. 25, pp. 865 – 885.

(Landsea et al., 2014)
Landsea, C. W. et al., (2014). The revised Atlantic hurricane database (HURDAT2). National Oceanic & Atmospheric Administration: National Hurricane Center. Retrieved from http://www.aoml.noaa.gov/hrd/hurdat/newhurdat-format.pdf

(Lipscy et al., 2013)
Lipscy, P. et al., (2013). The Fukushima disaster and Japan's nuclear plant vulnerability in comparative perspective. *Environ. Sci. Technol.*, Vol. 47, Iss. 12, pp. 6082 – 6088.

(Luettich Jr. et al., 1992)
Luettich Jr., R. A. et al., (1992). ADCIRC: An advanced three-dimensional circulation model for shelves, coasts, & estuaries. Report 1 – Theory & methodology of ADCIRC-2DDI & ADCIRC-3DL. *Dredging Research Program*. Technical Report DRP-92-6. 137 pp.

(McAdie et al., 2009)
McAdie, C. J., et al., (2009). Tropical cyclones of the North Atlantic Ocean, 1871 – 1998 (6th revision with 2007 & 2008 track maps included). DOC/NOAA. *Hist. Clim. Ser. 6-2*.

(Massey, et al., 2011)
Massey, T. et al., (2011). Coastal Storm Modeling-System Integration. *Sol. to Cst. Dis.* Pp. 99 – 108.

(McClave & Sincich, 2009)
McClave, J. T., Sincich, T., (2009). Statistics. Upper Saddle River, New Jersey: Pearson Education, Inc. 11th Ed., pp. 781 – 812.

(Myers, 1954)
Myers, V. A., (1954). Characteristics of United States hurricanes pertinent to levee design for Lake Okeechobee, Florida. *The Hydrometeor. Rep. No. 32*.

(Myers, 1970)
Myers, V. A., (1970). Joint probability of tide frequency analysis applied to Atlantic City and Long Beach Island, NJ. ESSA Tech Memo WBTM Hydro – 11.

(NASA, 2015)
National Aeronautics & Space Administration, (2015). How do hurricanes form? Retrieved from http://spaceplace.nasa.gov/hurricanes/en/

(NOAA, 2005)
National Oceanic & Atmospheric Administration: National Weather Service, (2005). National Hurricane Center: The great New England hurricane of 1938. Retrieved from http://www.erh.noaa.gov/box/hurricane/hurricane1938.shtml

(NOAA, 2013)
National Oceanic & Atmospheric Administration: Tides & Currents, (2013). Mean sea level trend at The Battery, NY. Retrieved from http://tidesandcurrents.noaa.gov/sltrends/sltrends_station.shtml?stnid=8518750

(NOAA, 2014)
National Oceanic & Atmospheric Administration: National Weather Service, (2014). National Hurricane Center: Revised Atlantic hurricane database (HURDAT2). Retrieved from http://www.nhc.noaa.gov/

(NOAA, 2015)
National Oceanic & Atmospheric Administration: National Weather Service, (2015). Tides & Currents: Datum values for 8518750, The Battery, NY. Retrieved 2015. Retrieved from http://tidesandcurrents.noaa.gov/datums.html?id=8518750

(NYC, 2014)
The City of New York, (2014). 2014 New York City hazard mitigation plan. Office of Emergency Management.

(Niedoroda et al., 2008)
(Niedoroda A. W. et al., (2008). Efficient strategies for the joint probability evaluation of storm surge hazards. *Sol. to Cst. Dis.* Pp. 242 – 255.

(Niedoroda et al., 2010)
Niedoroda, A. W. et al., (2010). Analysis of the coastal Mississippi storm surge hazard. *J. Ocean Engr.*, Vol. 37, Iss. 1, pp. 82 – 90.

(Powell & Reinhold, 2007)
Powell, M. D., Reinhold, T. A., (2007). Tropical cyclone destructive potential by integrated kinetic energy. *Bull. Amer. Meteor. Soc.*, Vol. 88, Iss. 4, pp. 513 – 526.

(Resio, 2007)
Resio, D. T., (2007). White paper on estimating hurricane inundation probabilities. Engineer Research and Development Center (ERDC), US Army Corps of Engineers, Vicksburg, MS.

(Resio et al., 2009)
Resio, D. T. et al., (2009). A surge response function approach to coastal hazard assessment – Part 1: Basic concepts. *J. Nat. Haz.*, Vol. 51, Iss. 1, pp. 163 – 182.

(Resio et al., 2013)
Resio, D. T. et al., (2013). The effect of uncertainty on estimates of hurricane surge hazards. *J. Nat. Haz.*, Vol. 66, Iss. 3, pp. 1443 – 1459.

(Resio & Irish, 2015)
Resio, D. T., Irish, J. L., (2015). Tropical cyclone surge risk. *Curr. Clim. Chng. Rpts.* In press.

(Schwerdt et al., 1979)
Schwerdt, R. W. et al., (1979). Meteorological criteria for standard project hurricane and probable maximum hurricane wind fields, Gulf & East Coasts of the United States. *NOAA Tech. Rep – NWS 23*. 316 pp.

(Scotti, 2003)
Scotti, R. A., (2003). Sudden Sea: The Great Hurricane of 1938. Boston, Massachusetts. Little, Brown, & Co.

(Tarbuck & Lutgens, 2006)
Tarbuck, E. J., Lutgens, F. K., (2006). Earth science. Upper Saddle River, New Jersey: Pearson Education, Inc. 11th Ed., pp. 402 – 535.

(Toro et al., 2010a)
Toro, G. R. et al., (2010). Quadrature-based approach for the efficient evaluation of surge hazard. *J. Ocean Engr.*, Vol. 37, Iss. 1, pp. 114 – 124.

(Toro et al., 2010b)
Toro, G. R. et al., (2010). Efficient joint probability methods for hurricane surge frequency analysis. *J. Ocean Engr.*, Vol. 37, Iss. 1, pp. 125 – 134.

(Toro, 2012)
Toro, G. R., (2012) Operating guidance no. 8 – 12 for use by FEMA staff and flood hazard mapping parameters.

(Uhlhorn & Black, 2003)
Uhlhorn, E. W., Black, P. G., (2003). Verification of remotely sensed sea surface winds in hurricanes. J. Atmos. O. Tech., Vol. 20, Iss. 1, pp. 99 – 116.

(USGS, 2014a)
United States Geological Survey, (2014). St. Petersburg coastal and marine science center. Coastal change hazards: Hurricanes and extreme storms. Retrieved from http://coastal .er.usgs.gov/hurricanes/extreme-storms/northeaster.php

(USGS, 2014b)
United States Geological Survey, (2014). St. Petersburg coastal and marine science center. Coastal change hazards: Hurricanes and extreme storms. Retrieved from http://coastal .er.usgs.gov/hurricanes/extreme-storms/hurricanes.php

(Velden et al., 1997)
Velden, C. et al., (1997). Development of an objective scheme to estimate tropical cyclone intensity from digital geostationary satellite infrared imagery. *Weath. Forecast.* Vol. 13, pp. 172 – 186.

(Velden et al., 2006)
Velden, C. et al., (2006). The Dvorak tropical cyclone intensity estimation technique: A satellite-based method that has endured for over 30 years. *Bull. Amer. Meteor. Soc.*, Vol. 87, Iss. 9, pp. 1195 – 1210.

(Vickery et al., 2000)
Vickery, P. J. et al., (2000). Simulation of hurricane risk in the U.S. using the empirical track model. *J. Strct. Engr.*, Vol. 126, Iss. 10, pp. 1222 – 1237.

(Vickery & Wadhera, 2008)
Vickery, P. J., Wadhera, D., (2008). Statistical models of Holland pressure profile parameter & radius to maximum winds of hurricanes from flight-level pressure & H*Wind Data. *J. App. Meteor. & Clim*. Vol. 47, pp. 2497 – 2517.

(Westerink & Luettich Jr. 1994)
Westerink, J. J., Luettich Jr., R. A., (1994). Meshing requirements for large scale coastal ocean tidal models. Proceedings of the X International Conference on Computational Methods in Water Resources, A. Peters et al. Eds., Heidelberg, Germany. Pp. 1323 – 1330.

VITA

Hunter Bredesen currently has a Bachelor of Science in Civil Engineering degree from the University of North Florida (UNF), which was awarded to him in 2012. While pursuing his degrees, Mr. Bredesen worked part-time as a civil engineering intern for Civil Services, Inc. in Jacksonville, Florida. He became a field and specimen testing technician with the American Concrete Institute in 2010 and participated in different student organizations such as Engineers Without Borders and the American Society of Civil Engineers.

Mr. Bredesen was immediately hired by a consulting engineering firm, Taylor Engineering, Inc. (Taylor), after graduating from UNF in 2012. While working as a coastal engineering intern for Taylor, he was accepted to the Coastal Engineering Department by the UNF Graduate School. Over the past three years, Mr. Bredesen worked as a graduate assistant in that department and as an intern at Taylor. He founded the student chapter engineering society Coasts, Oceans, Ports, and Rivers Institute in the fall of 2012 and held a presidential role over the 2012-13 academic year. He has maintained a 3.78 graduate grade point average and anticipates graduating with a Master of Science in Coastal Engineering degree in May, 2015.

Dr. Don Resio of UNF serves as Mr. Bredesen's academic advisor. Both were eager to share the accumulation of work that he accomplished over the 2014-15 academic year, which is presented herein.